A common analgesic enhances the anti-tumour activity of 5-aza-2'-deoxycytidine through induction of oxidative stress

Hannah J. Gleneadie[1,10], Amy H. Baker[1], Nikolaos Batis[2], Jennifer Bryant[2], Yao Jiang[3], Samuel J.H. Clokie[4], Hisham Mehanna[2], Paloma Garcia[5], Deena M.A. Gendoo[6], Sally Roberts[5], Alfredo A. Molinolo[7], J. Silvio Gutkind[8], Ben A. Scheven[1], Paul R. Cooper[1], Farhat L. Khanim[9] and Malgorzata Wiench[1, 5,*].

[1]School of Dentistry, Institute of Clinical Studies, College of Medical and Dental Sciences, The University of Birmingham, Birmingham, B5 7EG, UK; [2]Institute of Head and Neck Studies and Education (InHANSE), The University of Birmingham, Birmingham, B15 2TT, UK; [3]School of Biosciences, The University of Birmingham, Birmingham, B15 2TT, UK; [4]West Midlands Regional Genetics Laboratory, Birmingham Women's and Children's Hospital, Birmingham, B15 2TG, UK; [5]Institute of Cancer and Genomic Sciences, College of Medical and Dental Sciences, The University of Birmingham, Birmingham, B15 2TT, UK; [6]Centre for Computational Biology, Institute of Cancer and Genomic Sciences, The University of Birmingham, Birmingham, B15 2TT, UK; [7]Moores Cancer Center and Department of Pathology, University of California San Diego, La Jolla, CA 92093, USA; [8]Department of Pharmacology and Moores Cancer Center, University of California San Diego, La Jolla, CA 92093, USA; [9]Institute of Clinical Studies, University of Birmingham, Birmingham B15 2TT, UK, [10]Present address: MRC London Institute of Medical Sciences, Imperial College London, London, W12 0NN, UK

*Correspondence: Malgorzata Wiench, School of Dentistry, Institute of Clinical Studies, Institute of Cancer and Genomic Sciences, The University of Birmingham, 5 Mill Pool Way, Birmingham B5 7EG, Tel: +44 (0) 1214665520, m.d.wiench@bham.ac.uk

Running title: Paracetamol sensitizes cancer cells to DAC

Financial support: This research was supported by grants from the FP7 Framework Marie Curie Actions CIG (methDRE) to M. Wiench and The Royal Society (RS-9-10-2012) to M. Wiench. H.J. Gleneadie received a joint University of Birmingham and Medical Research Council UK fellowship.

Character count (with spaces): 70,503

Abstract

The DNA demethylating agent 5-aza-2'-deoxycytidine (DAC) has anti-cancer therapeutic potential, but its clinical efficacy is hindered by DNA damage-related side effects and its use in solid tumours is debated. Here we describe how common analgesic paracetamol can augment the effects of DAC on cancer cell proliferation and differentiation, without enhancing DNA damage. Firstly, DAC treatment specifically upregulates cyclooxygenase-2-prostaglandin E_2 pathway, inadvertently providing cancer cells with survival potential, while the addition of paracetamol offsets this effect. Secondly, in the presence of paracetamol, DAC leads to glutathione depletion and ROS accumulation. Finally, this oxidative stress is further enhanced by DAC suppressing anti-oxidant and thioredoxin responses. Analyses of TCGA datasets show that the DAC/paracetamol combination targets pathways of clinical importance in many cancers. The benefits of combined treatment are demonstrated here in head and neck squamous cell carcinoma (HNSCC) and acute myeloid leukaemia cell lines and corroborated in a HNSCC xenograft mouse model. In summary, paracetamol increases DAC efficacy such that it could be used at clinically relevant doses; providing a strong rationale for consideration in cancer therapy.

Keywords: 5-aza-2'-deoxycytidine/acute myeloid leukemia/epigenetic therapies/head and neck squamous cell carcinoma/paracetamol

Introduction

Aberrant DNA methylation patterns are common in most cancers, arise early in tumour development and are potentially reversible by hypomethylating agents (Jones & Baylin, 2002). The DNA demethylating agent 5-aza-2'-deoxycytidine (Decitabine or DAC) is a nucleoside analogue that incorporates into replicating DNA in place of cytosine where it traps and promotes the degradation of DNA methyltransferases (DNMTs) (Stresemann & Lyko, 2008). This results in two anti-cancer activities: methyl marks cannot be copied during DNA replication causing widespread DNA demethylation and adducts are formed in the DNA leading to DNA damage and apoptosis (Stresemann & Lyko, 2008). DAC has been approved by the European Medicines Agency (EMA) for treatment of acute myeloid leukaemia (AML) (Kantarjian *et al*, 2012; Nieto *et al*, 2016). Pre-clinical studies suggest it might also be effective in solid tumours (Tsai *et al*, 2012), athough the outcomes of clinical trials are highly

variable (Linnekamp *et al*, 2017). DNA demethylating drugs are thought to de-repress epigenetically silenced tumour suppressor genes as well as demethylate endogenous retroviruses (ERVs), triggering an antiviral immune response and cancer cell death (Chiappinelli *et al*, 2015; Roulois *et al*, 2015; Stresemann & Lyko, 2008).

Head and neck squamous cell carcinoma (HNSCC), the 6th most common cancer worldwide, has 5-year survival rates of ≤40%, highlighting a pressing need for new therapies (Simard *et al*, 2014).The tumours originate from stratified squamous epithelium of the oral cavity and pharynx where the cells in the basal cell layer proliferate and replenish the suprabasal layers which undergo terminal differentiation (Squier & Kremer, 2001). Although DNA methylation aberrations are common in HNSCC (Steinmann *et al*, 2009) the clinical evaluation of DAC potential in HNSCC is very limited (Abele *et al*, 1987).

In solid tumours, DAC alone may not be curative, but favourable effects were observed for epigenetic agents combined with other chemo- and immune-therapies (Linnekamp *et al.*, 2017). So far it has not been explored whether the response to DAC could be enhanced by other compounds, not traditionally used in cancer treatment. In the current study, a custom-built library of 100-commonly used, cost-effective, off-patent drugs (Khanim *et al*, 2011) was investigated for their ability to sensitise HNSCC cells to DAC treatment. Of the drugs tested, paracetamol was identified to work in synergy with DAC.

Paracetamol (acetaminophen) is the most commonly used analgesic and antipyretic in both Europe and the United States, present on the market since the 1950s (Bertolini *et al*, 2006). Paracetamol affects the cyclooxygenase (COX) pathway wherein arachidonic acid (AA) is metabolized to prostaglandin H_2 (PGH_2) by either constitutively expressed COX-1 (PTGS1) or inducible COX-2 (PTGS2) (Graham *et al*, 2013). PGH_2 is then rapidly converted, by respective prostaglandin synthases, into effector prostanoids (prostaglandins PGE_2, PGF_2; PGI_2 and PGD_2 or thromboxane TXA) and these work, in part, through metabolite-specific G-protein coupled receptors to activate downstream pathways (Graham *et al.*, 2013). Additionally, other AA-derived metabolites are produced either through the lipoxygenase (LOX) or the monooxygenase (cytochrome P450) pathways (Wang & Dubois, 2010).

The COX-2-PGE_2 axis is associated with inflammation, growth and survival and is thought to contribute to the 'inflammogenesis of cancer' (Liu *et al*, 2015). Increased expression of COX-2 and production of PGE_2 are found in many solid tumours, including HNSCC, and correlate with tumour stage, metastasis and worse clinical outcome whilst low levels are

associated with better response to chemotherapy (Liu *et al.*, 2015; Saba *et al*, 2009). This pathway has also been implicated in the development of chemoresistance and linked to repopulation of cancer stem cells (Kurtova *et al*, 2015). Hence, COX-2 inhibitors have been tested for their therapeutic anti-cancer potential, showing protection against cancer development (Kim *et al*, 2010; Saba *et al.*, 2009). However, the only research that suggests paracetamol may have therapeutic potential in established tumours used overdose concentrations of the drug, either alone or in combination with other chemotherapeutics (Kobrinsky *et al*, 1996; Posadas *et al*, 2007; Wu *et al*, 2013).

Here we show that paracetamol can be used at clinically relevant concentrations to sensitize cancer cells (both HNSCC and AML) to DAC treatment, allowing for DAC dose-reduction.

Results

HNSCC cell lines show bimodal sensitivity to DAC treatment

To establish the potential of DAC as a therapeutic in HNSCC, relative cell viability was determined in four HNSCC cell lines and in normal human oral keratinocytes (HOK) after 96h of treatment (Fig 1A). HOK cells showed only moderate sensitivity to DAC treatment with no decrease in viability at clinically relevant concentrations and an IC_{50} of 8.93 µM. Interestingly, the four HNSCC cell lines could be divided into two distinct groups; DAC-sensitive (VU40T, IC_{50} of 2.17 µM and HN12, IC_{50} of 0.81 µM) and those with little (SCC040, IC_{50} of 10.61 µM) to no sensitivity (UDSCC2) (Fig 1A). This pattern was mirrored in the ability of DAC to demethylate DNA in the sensitive cell lines only (Fig 1B). These data suggest that the efficacy of DAC treatment is proportional to its ability to demethylate DNA, therefore likely dependent on cellular drug uptake, activation or retention.

Efficacy of DAC treatment can be synergistically increased with paracetamol

In patients with AML, a 5-day regimen of 20mg/m^2 DAC gave a maximum plasma concentration (Cmax) of 107 ng/ml, equivalent to 469 nM (European Medicines Agency, 2019; Nieto *et al.*, 2016), while all HNSCC cell lines have an IC_{50} value greater than 500 nM. Therefore, one sensitive (VU40T) and one resistant (SCC040) cell line were subjected to DAC sensitising screen to establish whether the efficacy of DAC could be increased (Fig 1C, Appendix Fig S1). The cells were treated with 500 nM DAC with or without one of a panel of 100 off-patent drugs (drug repurposing library FMC1(Khanim *et al.*, 2011)) and compared to the drug-only control. In the resistant SCC040 cells, none of the drugs were able to

sensitize the cells to DAC (Appendix Fig S1A). However, in the DAC-sensitive VU40T cell line, paracetamol, valproic acid (VPA) and zinc acetate further decreased cell viability (Fig 1C, Appendix Fig S1B). The paracetamol effect was replicated in the remaining cell lines: the efficacy of DAC was increased by paracetamol and zinc acetate in DAC-sensitive HN12 but not in DAC-resistant UDSCC2 cells (Fig 1D). Importantly, paracetamol alone did not alter the viability of HOK cells which were otherwise highly sensitive to both VPA and zinc acetate (Fig 1D). Therefore, DAC-paracetamol combination was further tested for synergy in VU40T and HN12 cells using the Chou-Talalay method (Chou, 2006). The cell viability was assessed in response to each drug separately and in combination across eight constant-ratio matched titration of Cmax (500 nM for DAC and 132 µM for paracetamol) (Fig 1E-F). This analysis showed combination index (CI) values less than 1 at all bar the lowest concentration, demonstrating synergy of supra-additive nature (Fig 1G). In VU40T cells, the dose reduction index (DRI) indicated that almost 5 times less of each drug could be used when applied in combination (Appendix Table S1), allowing DAC dose reduction from 2.26 µM to the clinically relevant 450 nM (European Medicines Agency, 2019; Nieto *et al.*, 2016). A similar reduction was observed for HN12 cells (Appendix Table S2).

Combined DAC-paracetamol treatment augments the effects of DAC on cell metabolism, proliferation and markers of basal epithelial cells

In DAC-responsive VU40T cells the combined DAC-paracetamol treatment decreased cell number compared to DAC alone (Fig 2A). It was next investigated whether the underlying mechanisms involved reduced proliferation, altered cell cycle progression or increased cell death, possibly due to enhanced DNA damage.

DAC is known to cause cell death and DNA damage (Stresemann & Lyko, 2008). As expected, 500 nM DAC increased both apoptosis and necrosis as shown by annexin V and propidium iodide staining but this was not altered by the addition of paracetamol (Fig 2A-B). Similarly, in VU40T cells, DAC treatment significantly increased DNA damage and double strand breaks as highlighted by an increase in the number of nuclei with γH2AX foci when compared to control; however, this too was not additionally enhanced by combined treatment (Fig 2C).

When compared to untreated cells none of the treatments resulted in change in cell cycle progression, however, the addition of paracetamol to DAC treatment led to fewer cells progressing to G2/M phase than for DAC alone (Fig 2D). This additional effect of

paracetamol was also observed for cell proliferation. Treatment with 500 nM DAC reduced the number of Ki67 positive nuclei and combined treatment further decreased their number, whilst paracetamol alone had no effect (Fig 2A and E). Furthermore, markers for the basal cell layer (the only cell layer in stratified epithelium that normally contains dividing cells), *TP63* and keratin 5 (*KRT5*), were down-regulated by DAC in a dose-dependent manner and this was enhanced by DAC-paracetamol combined treatment (Fig 2F). Notably, TP63 is a key transcription factor in stratified epithelium (Yoh & Prywes, 2015) and its overexpression and/or amplification is observed in ~ 30% of tumours in the TCGA HNSCC cohort (Appendix Fig S2). Conversely, involucrin (*IVL*), a marker for differentiated, suprabasal layers was upregulated upon DAC and even more so by DAC-paracetamol treatments (Fig 2G).

RNA sequencing performed on the DAC-sensitive VU40T cells demonstrated that DAC treatment substantially altered the transcriptome while paracetamol alone only resulted in modest changes (Fig 2H). However, addition of paracetamol to DAC treatment resulted in significantly greater changes in gene expression compared to DAC alone (Fig 2H). Six gene sets, up- and down-regulated by each treatment (Fig 2H, Appendix Table S3), were subjected to gene set enrichment analysis using GO Biological Processes (Ashburner *et al*, 2000) and consolidated in REVIGO (Supek *et al*, 2011) (Fig 2I, Appendix Table S4). Paracetamol treatment alone resulted in no significant enrichment for down-regulated gene sets; treatment primarily resulted in up-regulation of genes involved in respiratory electron transport chain. The profile upregulated by DAC was dominated by immune terms, especially interferon type I response. This was also evident in the combined treatment, although to a lesser extent. Interestingly, combined treatment was enriched for terms related to tissue development and differentiation (including 'pharyngeal system development' Appendix Table S4), confirming the possible change from basal cell-like to more differentiated epithelial cell phenotype. Genes down-regulated by both DAC and DAC+paracetamol showed similar ontology groupings related to DNA, protein and RNA metabolism but the enrichment was much stronger for the combined treatment (Fig 2I) due to higher number of differentially regulated genes (Fig 2H). This suggests that the addition of paracetamol to DAC significantly amplifies decreases in metabolism and DNA replication caused by DAC alone.

Therefore, although DAC alone has profound effects on proliferation, differentiation, cell death and DNA damage, the further reduction in viability observed after the addition of

paracetamol appears to be associated with decreased proliferation and divergence from the basal cell-like phenotype.

DAC treatment enhances the cyclooxygenase pathway, which is offset by paracetamol

Paracetamol is understood to act on the cyclooxygenase pathway, primarily through inhibition of COX-2 (PTGS2) (Graham *et al.*, 2013). Notably, a geneset for 'Prostanoid biosynthetic process' was enriched after both DAC and combined treatments (Appendix Table S4). Therefore, the effect of DAC on this pathway was further examined. In DAC-sensitive cell lines only, *PTGS2* RNA and protein levels were upregulated following DAC treatment and this was maintained after combined treatment (Fig 3A and B). A corresponding increase in the downstream product, prostaglandin E_2 (PGE_2), was observed in the DAC-sensitive VU40T cells but not in the resistant SCC040 cells (Fig 3C). PGE_2 returned to basal levels by the addition of 132 µM paracetamol (Fig 3C) which indicates that paracetamol dampens DAC-induced COX-2 pathway activation. In addition, expression of the PGE_2 receptors *PTGER1* and *PTGER2* increased in the DAC-sensitive cells VU40T and HN12, respectively, whilst no significant changes in *PTGER1-4* expression occurred in the DAC-resistant cells UDSCC2 and SCC040 (Fig 3D and Appendix Fig S3A). Transcriptional activation of the COX-2-PGE_2 pathway by DAC was evident in the RNA-seq data, together with COX-2-TXA_2, whilst the PGF_2, PGI_2 and PGD_2, pathways were not upregulated (Appendix Fig S3B and C). In summary, DAC treatment specifically upregulates many aspects of the COX-2-PGE_2 pathway, inadvertently providing the cancer cells with growth and survival potential, while the addition of paracetamol offsets this effect (Fig 3E).

There is a possibility that blocking the COX pathway with paracetamol could shunt AA towards the LOX pathway also leading to increased survival potential (Park *et al*, 2012). DAC treatment altered gene expression of enzymes involved in the LOX pathway by both up- (*ALOX5* and *ALOX15B*) and down- (*LT4H* and *ALOX12*) regulating them (Appendix Fig S3D). However, the secretion of cysteinyl leukotrienes and leukotriene B_4 remained below levels detectable by ELISA in all experimental conditions in VU40T and SCC040 cells. Therefore, there is no indication for LOX pathway compensation following COX-2 inhibition by paracetamol in the cell lines examined, although the involvement of other metabolites cannot be excluded (Appendix Fig S3E).

DAC treatment complements cancer-related activation of COX-2-PGE_2 pathway

Activation of the COX-2-PGE_2 pathway has been previously indicated in both HNSCC and other cancer types (Liu *et al.*, 2015; Saba *et al.*, 2009). In the most recent TCGA cohort, 29% of HNSCC tumours (150/520 patients) have at least one component of COX-2-PGE_2 pathway transcriptionally activated: mostly through upregulation of PGE_2 synthases or PGE_2 receptors (Fig 3F). Similar activation can be observed in other cancers (Appendix Table S5). However, over-expression of *PTGS2* itself is relatively rare (2.3% in HNSCC, Fig 3F), potentially serving as a limiting factor in the full activation of the pathway. Therefore, the DAC-induced upregulation of *PTGS2* could remove this limitation and counteract the anti-tumour effects of DAC. This mechanism could be applicable to other tumour types; *PTGS2* up-regulation by DAC was detected by Drug Perturbation Signatures (Fig 3G) from the cMAP dataset (Lamb *et al*, 2006) indicating the wider potential of DAC-paracetamol co-treatment.

Combined treatment mimics the effects of paracetamol overdose and depletes glutathione levels

If COX-2-PGE_2 pathway alterations were to be solely responsible for the synergy between DAC and paracetamol, other COX inhibitors should have a similar effect. However, neither the generic COX inhibitor ibuprofen, nor the COX-2 specific inhibitor valdecoxib sensitized HNSCC cells to DAC treatment (Fig 4A, Appendix Fig S4), despite valdecoxib being able to reduce DAC-stimulated PGE_2 production to a similar extent as paracetamol (Fig 4B). This suggests an additional, paracetamol-specific, mechanism accounts for the synergistic relationship between DAC and paracetamol.

Previous work on the anti-cancer therapeutic potential of paracetamol involved toxic doses of the drug (Kobrinsky *et al.*, 1996; Posadas *et al.*, 2007; Wu *et al.*, 2013). Efficacy was attributed to an accumulation of toxic metabolite of paracetamol, N-acetyl-p-benzoquinone-imine (NAPQI), resulting in glutathione depletion (Kobrinsky *et al.*, 1996; Posadas *et al.*, 2007; Wu *et al.*, 2013) (Fig 4C). By comparison, our current work was performed using a safe, clinically achievable serum concentration of paracetamol (132 µM) . However, in DAC-sensitive VU40T cells, DAC treatment caused an increase in the CYP450 enzyme, *CYP2E1*, thought to be primarily responsible for the conversion of paracetamol into NAPQI (Fig 4D-E). Assessing NAPQI levels is unreliable due to its highly reactive nature (Dahlin *et al*, 1984). However, combined treatment led to a dramatic reduction in GSH levels, a surrogate marker often used, and the effect was equivalent to a high dose (1mM) paracetamol (Fig 4F). Furthermore, N-acetyl cysteine (NAC) is clinically used as an antidote to treat paracetamol overdose by replenishing GSH and preventing NAPQI accumulation (Kobrinsky *et al.*, 1996).

In VU40T cells, 48h pre-treatment with 2.5 mM NAC led to increased cell viability in all conditions, but significantly and to the greatest extent in the DAC+paracetamol treated cells, where viability was restored to the control level (Fig 4G). Therefore, the combined treatment mimics the effects of paracetamol overdose at therapeutic concentrations and depletes GSH stores in tumour cells.

GSH is an intracellular antioxidant that acts primarily as a reactive oxygen species (ROS) scavenger (Forman *et al*, 2009). In agreement with this, DAC-paracetamol co-treatment significantly increased both intracellular ROS (Fig 4H) and mitochondrial superoxide (Fig 4I) as compared to DAC alone. This was specific for DAC co-treatment with paracetamol and not valdecoxib (Fig 4H-I). Accumulation of ROS typically triggers an anti-oxidant response which can protect cancer cells treated with chemotherapeutics (Ray *et al*, 2012). However, upon both DAC and DAC-paracetamol treatment the majority of genes described as direct anti-oxidant responders (Raghunath *et al*, 2018) are down-regulated (Fig 4J). Therefore, the transcriptional anti-ROS response is impaired by DAC treatment which leads to further exacerbation of oxidative stress and decreased cancer cell survival. Finally, it has been shown that keratinocytes can tolerate GSH depletion as long as the cysteine pools (uptake of cystine by SLC7A11 or cysteine by SLC1A4) and the thioredoxin reductase system (TXN/TXNRD) are functional (Telorack *et al*, 2016). Again, DAC downregulated the majority of these genes which would inhibit this compensating mechanism (Fig 4K).

To summarize, in cancer cells DAC-paracetamol co-treatment mimics the mechanisms of paracetamol overdose, whilst cell adaptation to oxidative stress is impaired by DAC (Fig 4L). The specificity of the DAC-paracetamol interaction is further supported through Drug Set Enrichment Analysis (DSEA). The DSEA algorithm aims to identify the mechanisms of action shared by a set of drugs (Napolitano *et al*, 2016). Indeed, DAC and paracetamol share significant enrichment for COX, cytochrome P450 and GSH metabolism pathways, while this was not observed for DAC and valdecoxib combination (Fig 4M, Appendix Fig S5). Interestingly, the analysis also indicated high enrichment for genes attributed to keratinocyte differentiation (Fig 4M).

DAC-paracetamol affected pathways contribute to HNSCC patients' survival

The mechanisms underlying the efficacy of DAC-paracetamol co-treatment identified so far are multifactorial (Fig 5A). Firstly, the COX-2-PGE_2 pathway is specifically upregulated by DAC, potentially improving cancer cells survival. Indeed, when upregulated, this pathway

negatively affects HNSCC patient survival (Fig 5B). This is specific to COX-2-PGE_2 but not to other COX pathways or to the LOX pathway (Appendix Fig S6A and B). The addition of paracetamol to DAC treatment counteracts the induction of this pro-survival mechanism. Secondly, combined treatment leads to depletion of glutathione stores followed by oxidative stress, both of which restrict tumour growth and improve the efficacy of anti-cancer drugs (Traverso *et al*, 2013). Therefore, in the proposed scenario, GSH is required to maintain cancer cell fitness. In agreement with this, genes involved in maintaining GSH stores are linked to poorer patients' survival in the TCGA cohort of HNSCC tumours (Fig 5C) as well as other cancers (Appendix Table S6). Thirdly, DAC treatment transcriptionally down-regulates anti-oxidant and thioredoxin responses known to prevent cellular adaptation to oxidative stress and protection from oxidative damage. Again, upregulation of these pathways, particularly the thioredoxin response, correlates with decreased survival of HNSCC patients (Fig 5D). These results suggest that the DAC-paracetamol combination targets pathways and genes of clinical importance in HNSCC patients.

In vivo potential of DAC-paracetamol combination treatment

An NSG mouse xenograft model using human HNSCC FaDu cells previously used in drug efficacy studies (Bryant *et al*, 2019) was utilized to assess the DAC-paracetamol treatment *in vivo.* Like HN12 and VU40T, FaDu cells showed high supra-additive effects for combined treatment (Fig 6A and B). Mice were injected with FaDu cells and the treatments (DAC, paracetamol, DAC+paracetamol or vehicle (PBS)) were administered 5 days a week (Fig 6C). After the first two weeks, tumours in the control and paracetamol-treated groups reached the maximum permissible size, while DAC alone and DAC+paracetamol groups were treated for another week (Fig 6C). Due to the strong initial response to DAC, the treatment was carried out with reduced DAC concentration (0.2 mg/kg). Although DAC alone showed a strong anti-tumour effect, the DAC-paracetamol treated tumours remained consistently smaller throughout the duration of the treatment (Fig 6C and D). No tumours from the DAC-paracetamol treated group exceeded 300 mm^3 (Fig 6E) and 5/6 animals survived until the end of the experiment at which point they started losing weight (Appendix Fig S7). Transcript analysis of RNA extracted from tumour tissue showed alterations consistent with the mechanism of DAC-paracetamol synergy: upregulation of *PTGS2* and *CYP2E1* (Fig 6F) and down-regulation of *TP63* and *KRT5* (Fig 6G).

Synergistic effects of DAC-paracetamol co-treatment are present in AML cell lines

Currently, DAC only has EMA approval in the treatment of AML (Nieto *et al.*, 2016). Therefore, combined treatment of DAC plus paracetamol was tested in two AML cell lines, SKM-1 and HL-60. The cells were treated for 72h and the drugs were found to work synergistically in both of them (Fig 7A-C). The combined effect was even more apparent after prolonged culture, which aimed to mimic the DAC treatment regimen in AML patients (European Medicines Agency, 2019) where the cells were treated for 72h followed by 21 days withdrawal over four cycles (Fig 7D). The benefits of DAC-paracetamol treatment were more pronounced with each consecutive cycle and by the time the cells reached the fourth cycle they were still responding well to combined treatment while becoming resistant to DAC alone (Fig 7D).

Similar to HNSCC cells, DAC treatment in AML cell lines activated several aspects of COX-2-PGE_2 pathway including upregulation of *PTGS2* and PGE_2 receptors' expression (Fig 7E). Upregulation of *CYP2E1* following DAC treatment was also noted for SKM-1 cells (Fig 7F). Ultimately, DAC increased ROS and mitochondrial superoxide production in these AML cells and this was further significantly enhanced by the addition of paracetamol but not valdecoxib (Fig 7G and H).

In further agreement with the results obtained for HNSCC cells, combined treatment did not add to the cell death caused by DAC alone as assessed by annexin V (Fig 7I). There was also little change to cell cycle progression after DAC when compared to control while combined treatment increased the number of cells retained in S phase when compared to DAC alone (Fig 7J). Following DAC and DAC-paracetamol treatments, AML cells displayed an increase of myeloid differentiation marker *CD11b* (*ITGAM*) (Fig 7K). Although this was not significantly different between combined treatment and DAC alone the effects of DAC+paracetamol were more apparent when cell morphology was assessed and showed a change towards myelocyte with increased cytoplasm and a high number of vacuoles (Fig 7L). These data indicate that DAC-paracetamol synergy and the effect it has on oxidative stress could be applicable to blood malignancies, where DAC is an accepted and widely used therapeutic option.

Discussion

The search for new drugs to improve the poor survival rate of HNSCC is ongoing. Our preliminary results using four HNSCC cell lines and an *in vivo* mouse model show that DAC alone has therapeutic potential in HNSCC which involves type I interferon activation.

However, the response is variable as it has been observed for other solid tumours (Linnekamp *et al.*, 2017) and patient stratification will be necessary to identify the DAC-responders. Future studies will look for predictive biomarkers, however the results shown here are clear that sensitivity to DAC is primarily dependent upon the ability of DAC to demethylate the DNA, and therefore likely due to incorporation, activation or retention of the drug, as suggested previously (Qin *et al*, 2009; Wu *et al*, 2016). Furthermore, an initial response to DAC treatment was a prerequisite for synergy with paracetamol, therefore the co-treatment is dependent upon the DNA demethylating capacity of DAC.

This is the first study to identify that paracetamol can enhance the anti-tumour activity of DAC. There are two main translational impacts of the DAC-paracetamol combination. Our data strongly indicate that adding paracetamol to DAC treatment could significantly lower the DAC dose needed to achieve therapeutic effects, broadening DAC application. In addition, it opens a potential for DAC dose reduction therefore potentially reducing DNA damage-related side effects.

Paracetamol is routinely prescribed as an analgesic, however it has not been considered so far whether its use may influence, positively or negatively, the efficacy of chemotherapy regimens. This study highlights that uncontrolled use of paracetamol during cancer therapies and clinical trials could affect the outcomes and interpretation of the results. Hence, further studies are required to look at the impact of supportive care medication in oncology.

Considering both DAC and paracetamol have broad effects with many potential interactions, we investigated and identified key mechanisms within the AA metabolism pathway that could underlie the synergy (summarized in Fig 5A). Both our data and analysis of public databases point towards DAC explicitly upregulating COX-2-PGE_2 pathway, therefore providing cancer cells with survival advantage. This also reflects the previously reported bias in cancer cells towards PGE_2 production to the detriment of other prostaglandins (Cebola *et al*, 2015; Cebola & Peinado, 2012). It remains to be established whether the COX-2-PGE_2 pathway activation is a direct result of DNA demethylation or is rather due to indirect mechanisms (e.g. response to dsRNA, cytokines or growth factors).

Surprisingly, the synergistic effect observed for paracetamol could not be reproduced using other COX-2 inhibitors. The data indicate an alternative paracetamol-specific mechanism; DAC-induced mimicry of paracetamol overdose leading to GSH depletion and exacerbated oxidative stress in cancer cells, both of which have the potential to restrict tumour growth and

improve patient survival (Traverso *et al.*, 2013). These cytoprotective pathways are also involved in development of drug resistance, hence their suppression might account for the extended drug sensitivity observed in AML cells after combined treatment.

Response to DAC has a profound effect on the transcriptional programme in HNSCC cells which is dominated by activation of type I interferon and anti-viral pathways, agreeing with recent reports on the role of 'viral mimicry' in cancer treatment with demethylating agents (Chiappinelli *et al.*, 2015; Roulois *et al.*, 2015). These effects are maintained but not increased by combined treatment. Instead, addition of paracetamol to DAC treatment led to a decrease in DNA, RNA and protein metabolism, together with reduced proliferation and enhanced differentiation. Concurrently, a strong enrichment for 'keratinocyte differentiation' was noted in the DSEA dataset shared by DAC and paracetamol signatures. Further experiments are required to establish the exact mechanisms leading to the changes in cell proliferation and differentiation upon combined treatment and whether they are linked to alterations in COX2-PGE_2 pathway and/or to 'mimicry of paracetamol overdose'. One possibility involves the effects of AA metabolism and ROS on PI3K/Akt and MAPK pathways, the main proliferation drivers in HNSCC (Cancer Genome Atlas, 2015). In HNSCC, mutations in the AA pathway have been reported to downregulate PI3K/Akt signalling (Cancer Genome Atlas, 2015), while patients with activating *PIK3CA* mutations specifically benefited from regular use of NSAIDs (Hedberg *et al*, 2019); confirming the significance of AA and COX pathways in HNSCC development and treatment.

Results obtained for AML cells confirm similar genes and pathways are being affected and suggest wider clinical potential for the DAC-paracetamol synergy. This is of importance because DAC is an accepted therapeutic option in AML patients which could directly benefit from the addition of paracetamol to their treatment regime. Paracetamol is one of the most commonly used drugs, both prescribed and self-medicated. Therefore, considering the mechanisms described here, its interaction with other drugs, especially chemotherapeutics, should be taken into consideration in cancer treatment.

Materials and methods

Cell lines and culture conditions

Five human HNSCC cell lines were used: SCC040 (German Culture Collection, DSMZ (#ACC660)), FaDu (ATCC (HTB-43)), VU40T (Prof H. Joenje (VU University Medical

Centre, Amsterdam)), HN12 (Dr J.F. Ensley (Wayne State University, Detroit, MI)) and UDSCC2 (Dr Henning Bier (University of Duesseldorf, Germany)). The cell lines were authenticated using STR profiling (NorthGene, UK). All HNSCC cell lines were maintained in DMEM (Sigma- Aldrich) supplemented with 10% fetal bovine serum (FBS) (Sigma-Aldrich), 1% penicillin-streptomycin (Gibco), 4 mM L-glutamine (Sigma-Aldrich), 1X non-essential amino acids (Life Technologies) and 1 mM sodium pyruvate (Life Technologies). Primary human oral keratinocyte (HOK) cells were purchased from Caltag Medsystems and cultured over Poly-L-Lysine in Oral Keratinocyte Medium supplemented with 1% oral keratinocyte growth supplement (all purchased from ScienceCell) and 1% penicillin-streptomycin. Two AML cell lines were used: SKM-1 (from Dr Stefan Heinrichs, University of Essen, Germany) and HL-60 (ATCC (CCL-240)). Cells were cultured in RPMI1640 medium (ThermoFisher Scientific), supplemented with 15% FBS (Sigma-Aldrich), 1% L-glutamine and 1% penicillin-streptomycin. All cell lines were regularly tested for mycoplasma using MycoAlert (Lonza) and experiments were performed within 18 passages after thawing.

Drugs treatments

All drugs were purchased from Sigma-Aldrich. 5-Aza-2'-deoxycytidine (DAC) was dissolved in either 50% acetic acid or in ≥99.9% dimethyl sulfoxide (DMSO), all other drugs were dissolved in DMSO. The treatments were carried out for 96h (HNSCC cells) or 72h (AML cells) using a relevant vehicle as control.

Viability assay

Relative viability was determined in 96 well plates using the CellTiter-Blue Cell Viability Assay (Promega), including a minimum of triplicate wells per sample, vehicle, high concentration vehicle and 'media only' controls. Samples were normalised to a vehicle-only control. Sigma plot software (Systat Software Inc.) was used to generate sigmoidal, 4-parameter dose response curves after drug titrations. IC_{50} values were calculated using MyCurveFit (MyAssays Ltd.).

DAC sensitising assay

A panel of 100 drugs (Drug Library FMC1) were administered at the reported peak serum concentrations (Cmax) (Khanim *et al.*, 2011). Cells were seeded in 96-well plates and treated with each drug alone or in combination with 500 nM DAC. The assay was performed blind in biological triplicates with controls hidden within the panel.

Determining synergy

The Chou-Talalay method was employed to determine synergy (Chou, 2006) using constant-ratio matched titrations (0.125X, 0.25X, 0.5X, 1X, 2X, 3X, 4X, and 8X) of multiples of the Cmax (500 nM for DAC, 132 µM for paracetamol) and assessed by cell viability. The CompuSyn software (Chou, 2006) was used to calculate combination index (CI) and dose reduction index (DRI) values. CI values below 1 indicate synergy. DRI values indicate how many times less each drug can be used when in combination.

Long treatment of AML cells

SKM-1 and HL-60 cells were subjected to four cycles of 72h treatments followed by 21 days withdrawal period (details in Appendix Materials and Methods), the cells were counted at each passage using trypan blue (Sigma-Aldrich) staining and growth rates were calculated.

DNA dot blotting

DNA was extracted using the DNeasy Blood and Tissue Kit (Qiagen) and DNA dot blotting was performed as described in (Brown, 2001) using a titration of DNA; detailed protocol and antibodies are provided in Appendix Materials and Methods. Blots were normalized to methylene blue (Sigma-Aldrich) staining.

Western Blot analysis

WB analysis was performed as described previously (Khanim *et al.*, 2011), with some alterations; protocol details and antibodies are provided in Appendix Materials and Methods.

Giemsa-Jenner staining

VU40T cells were grown on coverslips for 96h, fixed in methanol and stained with Giemsa and Jenner (VWR) as previously described (Khanim *et al.*, 2011). SKM-1 cells were transferred to a glass slide with a Cytospin 3 (Thermo Shandon) before fixation. Microscope images were taken using EVOS XL Core Imaging System or BX-50 Olympus with a 100x oil immersion lens.

Immunofluorescence analysis

Immunofluorescence analysis was undertaken as described in (Roulois *et al.*, 2015) with details in Appendix Materials and Methods.

Apoptosis assay and cell cycle analysis

Apoptosis and necrosis were assessed using the Annexin V Apoptosis Detection APC kit (eBioscience, ThermoFisher Scientific) as the manufacturer recommends (see also Appendix

Materials and Methods). For cell cycle analysis, cells were fixed in 70% ice cold ethanol and resuspended in 200 µl 50 µg/ml propidium iodide solution (Sigma-Aldrich) and 50 µl of 100 µg/ml RNase solution (Roche). The solutions were analysed by flow cytometry on a Cyan B FACS analyser (Beckman Coulter).

ELISA

The levels of PGE_2, Leukotriene B_4 (LTB_4) and Cysteinyl leukotrienes (LTC_4, LTD_4, and LTE_4) were assessed in cell media using respective ELISA kits (Abcam). The results were normalised to the corresponding CellTiter-Blue viability results or cell count.

Determining glutathione concentration

The glutathione levels were measured using the GSH-Glo Glutathione Assay (Promega) with 1 mM paracetamol used as a positive control. The results were normalized against the corresponding CellTiter-Blue cell viability.

NAC rescue assay

N-acely-l-cysteine (NAC, Sigma-Aldrich) was dissolved in water and neutralised using 1 M sodium hydroxide (NaOH) (Sigma-Aldrich). VU40T cells were treated with 2.5 mM NAC or an equivalent volume of vehicle for 48h. Following this, wells were washed with fresh media and cells were treated with DAC, paracetamol or both for 96h and cell viability was determined.

Assessment of reactive oxygen species (ROS) and mitochondrial superoxide (mitosox)

MitoSOX Red (Cat# M36008, ThermoFisher Scientific) was used to assess mitosox, while ROS were measured using carboxy-H_2DCFDA (5-(and-6)-carboxy-2',7'-dichlorodihydrofluorescein diacetate, Cat# C369, Invitrogen), according to the manufacturers' protocols (details in Appendix Materials and Methods).

Real-Time Quantitative PCR (qRT-PCR)

Total RNA was extracted using RNeasy Mini Kit (Qiagen), including DNase I digestion step (RNase-Free DNase set, Qiagen). 1 µg of RNA was reverse transcribed (iScript cDNA Synthesis Kit (BioRad)) and the cDNA was purified with QiaQuick PCR Purification Kit (Qiagen). Purified cDNA was quantified using Qubit dsDNA High Sensitivity Assay kit (Thermo Fisher Scientific) to support normalization. qRT-PCRs were performed on a LightCycler 480 II using LightCycler 480 SYBR Green (Roche). Additional information and primers' sequences are provided in Appendix Materials and Methods.

RNA sequencing

For each sample three biological RNA replicates were pooled to make a library using the TruSeq Stranded mRNA Library Prep kit and sequenced using Illumina NextSeq 500 in paired-end mode at 2x75 bases in the Genomics Birmingham facility (Birmingham, UK). Reads were aligned to the genome (hg19) using HiSAT2 and processed with bedtools to generate normalised coverage plots. Details on quantification and data processing are in Appendix Materials and Methods.

Mouse xenograft study

The mouse xenograft study was performed as described previously (Bryant *et al.*, 2019) and details of the protocol are in Appendix Materials and Methods. To examine the toxicity and anti-tumour efficacy of DAC and paracetamol, we utilised male NOD/SCID/gamma (NSG) mice (Charles River) in accordance with the UK Home Office Animal (Scientific Procedures) Act 1986 and approved by the local University of Birmingham Ethical Review Committee. 24 males were implanted with $5x10^6$ FaDu HNSCC cells suspended in serum-free medium and injected subcutaneously into the right flank. After three days the tumours established and mice were randomly allocated into four treatment groups on a 5 day on, 2 day off regimen: 0.4 mg/kg DAC in PBS via IP injection (or 0.2 mg/kg in the week three); 1000 mg/kg paracetamol in PBS via oral gavage; DAC plus paracetamol as above; control (PBS) given both through the oral gavage and IP injection. Animals were monitored daily for signs of ill health and the tumours were measured. Upon culling, the tumours were excised and snap frozen for RNA extraction and subsequent analysis.

Quantification and statistical analysis

Statistical analysis and graphs were performed using GraphPad PRISM 8 software, unless stated otherwise. Details of the statistical tests used for each experiment are given in the corresponding figure legends.

TCGA data

Genetic alterations, gene expression and patient survival data were retrieved from The Cancer Genome Atlas (TCGA) via cBioPortal for Cancer Genomics (Gao *et al*, 2013); the details are described in Appendix Materials and Methods.

Drug perturbation signatures

Drug perturbation signatures were downloaded for the BROAD Connectivity Map dataset (CMAP) using the PharmacoGx package (version 1.14.0) (Smirnov *et al*, 2016) in R (details in Appendix Materials and Methods).

Drug Set Enrichment Analysis

The effect of Decitabine, paracetamol and valdecoxib drug combinations on KEGG pathways and Gene Ontology Biological Processes was conducted using the Drug Set Enrichment Analysis (DSEA) server (Napolitano *et al.*, 2016). Significance of the perturbed pathways of interest was identified using the corresponding p-values per geneset; $\log_{10}$ (p-values) were plotted as heatmaps.

Data availability

RNA-Seq data: The data are deposited at the GEO repository, accession number GSE110045 and SRA, accession number SRP132039.

Acknowledgments

We would like to thank Dr Jo Parish (University of Birmingham, UK) for critically reviewing the manuscript. This research was supported by grants from the FP7 Framework Marie Curie Actions CIG (methDRE) to M. Wiench and The Royal Society (RS-9-10-2012) to M. Wiench. H.J. Gleneadie received a joint University of Birmingham and Medical Research Council fellowship.

Author contributions

H.J.G., M.W., F.L.K., B.A.S., and P.R.C designed the project. H.J.G., M.W., and F.L.K. analysed the data. H.J.G. and M.W. performed most of the experiments in HNSCC cell lines. A.B. and P.G. performed most of the experiments in AML cell lines. N.B. designed and analysed drug synergy experiments. J.B. and N.B. performed *in vivo* experiments. Y.J. performed and analysed ROS and mitosox assays. S.C. analysed RNA-seq data. D.M.A.G. performed DSEA analysis. S.R., J.S.G. and A.M. provided essential advice and material. M.W. and H.J.G. wrote the manuscript with input from S.R., F.L.K., S.C. and H.M.

Conflict of interest

The authors declare no conflict of interest.

The paper explained

Problem

Aberrant DNA methylation patterns are common in most cancers, arise early in tumour development and are potentially reversible by hypomethylating agents. 5-aza-2-deoxycytidine (DAC) is a DNA methylation inhibitor currently approved for treatment of some haematological malignancies, however the efficacy of DAC in solid tumours remains unclear. We do not fully understand why some cancers have limited sensitivity to DAC, why the response is highly heterogenous in solid tumours and how, after the initial response, the cancer cells develop resistance to DAC. In addition, the clinical application of DAC is limited by cytotoxic side effects, mostly due to DNA damage. Therefore, the ability to lower the DAC dose to clinically safe levels would be of great clinical significance. Here we hypothesized that anti-tumour DAC effects can be enhanced through interaction with other, non-oncological, compounds. The DAC potential was initially tested in HNSCC, a cancer which originates from squamous epithelial lining of oral cavity and pharynx. HNSCC has very poor survival rates despite improved surgical and chemotherapy-based regimes, therefore new therapies are being sought for.

Results

By screening a panel of 100 off-patent drugs, paracetamol (acetaminophen) was identified to synergistically increase DAC response in HNSCC cells. This finding has been corroborated in HNSCC xenograft mouse models and in AML cells. The mechanisms for such interaction are multifactorial. Firstly, DAC upregulates cyclooxygenase COX-2-PGE_2 pathway inadvertently increasing cancer cell survival. This is counteracted by paracetamol, a known COX-2 inhibitor. Secondly, the combined treatment mimics the effects of paracetamol overdose and depletes GSH stores, which is followed by an increase in oxidative stress, both of which have the potential to restrict tumour growth and improve efficacy of anti-cancer drugs. We further show that cells are unable to protect themselves from this increased oxidative stress as both anti-oxidant and thioredoxin responses are impaired by DAC treatment. Ultimately, the combined DAC/paracetamol treatment leads to decreased cell metabolism and proliferation, as well as enhanced differentiation of cancer cells.

Impact

The study provides evidence that the anti-tumour potential of DAC can be enhanced by the presence of paracetamol applied in non-toxic doses, commonly used to alleviate pain. This has several clinical implications. The addition of paracetamol could allow for DAC dose reduction hence reducing DNA damage-related side effects and widening its clinical usability. In addition, the impact of anti-pain implementation in cancer therapy has not been systematically investigated and is not considered when planning treatments and clinical trials. Here we highlight the fact that the commonly used drug, available as over-the-counter medicine and often self-medicated by patients, can change the cancer cell response to a chemotherapeutic. The molecular pathways affected by the DAC/paracetamol co-treatment are shown to target vulnerabilities present across many tumour types, indicating wider potential for the drug combination. In HNSCC, DAC/paracetamol combination could have therapeutic potential in tumours susceptible to DACinduced DNA demethylation.

Figure legends

Figure 1 - DAC therapeutic potential in HNSCC cell lines can be synergistically increased by co-treatment with paracetamol.

A. Dose dependent cell viability in response to 96h DAC treatment in four HNSCC cell lines and normal oral keratinocytes (HOK). Grey box indicates clinically relevant doses.

B. Global levels of DNA methylation (5mC) analysed by DNA dot blot in HNSCC cell lines +/- 500 nM DAC, 96h. The data were normalized to methylene blue staining and an example of 5mC dot blot is shown below. For each replicate the results for 1 and 0.5 µg of DNA were averaged.

C. Scatterplot of the results from DAC sensitizing screen (full data in Appendix Fig S1) using 100 off patent drugs (Drug Library FMC1). Y axis represents increase in sensitivity, grey area shows ± 2SD.

D. Cell viability in HNSCC cell lines and HOK cells treated for 96h with 132.3 µM paracetamol (Para), 601.7 µM valproic acid (VPA) and 323.4 µM zinc acetate (Zinc) +/- 500 nM DAC. The results are independent confirmation of data shown in Fig 1C and Appendix Fig S2. Dotted lines show the effect of 500 nM DAC alone.

E-G. Synergy was determined using Chou-Talalay method. Cell viability data for VU40T (**E**) and HN12 (**F**) cells treated with fixed Cmax titrations of DAC (500 nM), paracetamol (132 µM) or DAC + paracetamol were used to calculate combination index (CI) (**G**) and dose reduction index (DRI) (Appendix Tables S1 and S2). CI <1 denotes synergy.

DAC-sensitive cell lines are shown in reds, resistant – in greys, HOKs – in blue.
Data information: In A-C and E-G n=3, in D n=7. In B statistical analysis was performed by paired two-tailed *t* tests. In D, for each cell line a matched One-Way ANOVA with Dunnett's multiple comparison testing was used to compare DAC to DAC+drug. A separate paired *t* test was applied to compare no treatment with DAC. Values are displayed as means ± SEM. Significant p values are shown.
Source data are available for this figure.

Figure 2 - DAC-paracetamol combination enhances the effects of DAC on cell metabolism, proliferation and basal cell phenotype.

A. Response of VU40T cells to paracetamol, DAC or both as indicated (representative images from 3 experiments). Left: Giemsa-Jenner staining (4x magnification); middle: Ki67 immunostaining; right: Annexin V and propidium iodine (PI) FACS analysis (healthy cells (bottom left); early apoptotic cells (bottom right); late apoptotic cells (top right) and necrotic cells (top left)).

B. Proportion of VU40T cells undergoing cell death assessed by FACS following Annexin V and PI staining (examples shown in (A)).

C. Percentage of VU40T nuclei with indicated numbers of γH2AX foci following indicated treatments.

D. Cell cycle distribution in VU40T cells following indicated treatments.

E. Proportion of VU40T nuclei positive for Ki67 immunostaining after indicated treatments (examples in (A)).

F. qRT-PCR for *TP63* and *KRT5* normalized to *ACTB* in VU40T cells treated as indicated.

G. qRT-PCR for *IVL* normalized to *ACTB* in VU40T cells treated as indicated.

H. Venn diagrams showing overlap for the most upregulated (left, $\log_2$ fold change ≥1) and down-regulated (right, $\log_2$ fold change ≤-1) genes as compared to vehicle control.

I. REVIGO-consolidated GO-BP pathways enriched for each indicated treatment. Top 5 terms from each group are included. Heatmap displays category scores as $\log_{10}$ p-value.

Data information: Unless stated otherwise all treatments were for 96h with 500 nM DAC and 132.2 µM paracetamol. In B-D and F-G n=3, in E n=6. In B and D: Two-Way ANOVA with Dunnett's correction was preformed to compare Ctrl with treatments and a separate Two-Way ANOVA with Sidak's was performed to compare DAC with combined treatment. In C: matched Two-Way ANOVA with Tukey's multiple comparison test was used to compare the

distribution of foci number between each treatment group. In E-G: matched One-Way ANOVA with Dunnett's multiple comparison test was used to compare all treatments to Ctrl. A separate paired two-tailed *t* test was used to compare DAC to DAC+paracetamol. Values are displayed as means ± SEM.

Figure 3 - DAC treatment specifically activates COX-2-PGE$_2$ pathway.

A. qRT-PCR for *PTGS2* in HNSCC cell lines treated as indicated. Data are shown as relative to vehicle control (Ctrl=1).

B. PTGS2 protein levels in VU40T and SCC040 cells. Graph represents the data from three experiments normalized to Lamin A/C.

C. PGE$_2$ concentration assessed by ELISA in media of VU40T and SCC040 cells treated for 96h as indicated. The data are normalized to cell viability.

D. qRT-PCR for PGE$_2$ receptors, *PTGER1* and *PTGER2*, shown as in (A).

E. Schematic of COX-2-PGE$_2$ pathway with confirmed DAC effects shown in red. COX-2 catalyzes the conversion of arachidonic acid into prostaglandin H$_2$. This is then converted into prostaglandin E$_2$ which exerts its effects through G-protein coupled receptors. The full COX-2 pathway is shown in Appendix Fig S3B.

F. COX-2-PGE$_2$-related gene expression across 522 HNSCC tumour samples. Heatmap created in cBioPortal based on provisional HNSCC cohort (TCGA). % indicates fraction of tumours with alterations.

G. Drug Perturbation Signature for genes of the COX-2-PGE$_2$ pathway for Decitabine (DAC) and paracetamol (Para) using cMap dataset.

Data information: Unless stated otherwise all treatments were for 96h with 500 nM DAC and 132.2 µM paracetamol and performed in three biological replicates. In A, B and D: for each cell line a matched One-Way ANOVA with Dunnett's multiple comparison test was used to compare all treatments to Ctrl; a separate paired two-tailed *t* test was used to compare DAC to DAC+paracetamol. In C: for each cell line an ordinary One-Way ANOVA with Sidak's correction was applied to compare treated groups with Ctrl. Values are displayed as means ± SEM. Only significant p-values are shown.

Source data are available for this figure.

Figure 4 - Combined DAC-paracetamol treatment mimics the effects of paracetamol overdose, depletes glutathione levels and leads to oxidative stress.

A. Cell viability in VU40T and HN12 cells treated for 96h with 132.3 µM paracetamol, 10

μM valdecoxib or 193.9 μM ibuprofen +/- 500nM DAC. Dotted line shows the effect of DAC alone.

B. PGE_2 concentration in the media of VU40T cells treated with DAC with or without paracetamol or valdecoxib shown as relative to either vehicle control (left) or DAC only treatment control (right).

C. Schematic of paracetamol overdose. A fraction of paracetamol is converted into the toxic metabolite NAPQI, and detoxified by GSH. When paracetamol is taken in excess GSH stores deplete and NAPQI accumulates.

D. qRT-PCR for *CYP2E1* in HNSCC cell lines treated as indicated and shown relative to vehicle control (Ctrl=1).

E. CYP2E1 protein levels in VU40T and SCC040 cells. The graph represents the data from three experiments normalized to Lamin A/C.

F. Glutathione (GSH) levels in VU40T cells treated with DAC, paracetamol or both, normalized to cell viability. 1 mM paracetamol was used as a positive control.

G. NAC rescue experiment. VU40T cells were pre-treated for 48h with 2.5 mM NAC followed by 96h of DAC, paracetamol or combined treatments and cell viability was assessed in comparison to control without NAC (left panel).

H. Levels of intracellular ROS (DCFDA staining and FACS) in VU40T cells treated for 72h as indicated. Upper figure: representative FACS profile; lower graph: geometric mean normalized to vehicle control.

I. Levels of mitochondrial superoxide were assessed as in (H) by MitoSOX Red staining.

J. Gene expression (RNA-seq data) of direct responders to oxidative stress shown as heatmap of $\log_2$ fold change values after indicated treatments.

K. Gene expression of cystin/TXN/TXNRD1 system components shown as in (J).

L. Schematic of proposed mechanism underlying DAC-paracetamol synergy: mimicry of paracetamol overdose leading to GSH depletion and oxidative stress. The effects of DAC are shown in red and paracetamol contribution – in blue.

M. Drug Set Enrichment Analysis for DAC, DAC + paracetamol, and DAC + valdecoxib combinations. Log_{10} p-values for selected pathways of interest (KEGG or GO BP genesets) are shown as heatmap.

Data information: Unless stated otherwise all treatments were for 96h with 500 nM DAC and 132.2 μM paracetamol, n=3 for A-B, D-F, H-I and n=4 for G. In A: for each cell line a mixed -effect analysis with Dunnett's correction was used to compare DAC to DAC+Vald and DAC+Ibup samples. In B, D-F: One-Way ANOVA with Dunnett's correction was used to

compare treatments with Ctrl. In D and F: a separate paired two-tailed *t* test was used to compare DAC to DAC+paracetamol. In G: for each group (+vehicle, +NAC) a matched One-Way ANOVA with Dunnett's was used to compare treatments with Ctrls; additionally, a paired two-tailed *t* test was used to compare Ctrl with NAC. In H-I: a matched One-Way ANOVA with Dunnett's correction was used to compare all groups to Ctrl; a separate ANOVA was used to compare DAC to DAC+Para and DAC+Vald. Values are displayed as means ± SEM. Only significant p values are shown.
Source data are available for this figure.

Figure 5 - Combined effects of DAC and paracetamol on AA metabolism and HNSCC patients' survival.

A. Arachidonic acid (AA) is metabolized to eicosanoids through COX, LOX, and cytochrome P450 monooxygenase pathways. In addition to DAC limiting cancer cell growth through either activation of tumour suppressor genes (TSGs) or viral mimicry (1), it inadvertently activates COX-2 PGE_2 pathway (2), which is contradicted by paracetamol. DAC also upregulates *CYP2E1* which, in the presence of paracetamol, leads to glutathione depletion and ROS accumulation, both enhanced by combined treatment (3). Simultaneously, DAC downregulates transcription of genes involved in antioxidant and thioredoxin responses, preventing cancer cells from developing adaptation to oxidative stress and protection from oxidative damage (4). GSH depletion has also potential to limit the production of LOX pathway metabolites dependent on GSH transferases.

B-D. Survival curves for 392 HNSCC patients with data available in TCGA provisional cohort with or without upregulation of genes (z-score ≥2.0) involved in indicated pathway. For gene sets see Appendix Materials and Methods. Kaplan Meier Estimates were plotted using cBioPortal. (**B**) Disease/ Progression-free survival curves for genes involved in COX-2-PGE_2 pathway. (**C**) Disease/Progression-free survival curves for genes involved in glutathione synthesis. (**D**) Disease/Progression-free survival curves for genes involved in antioxidant (left) and thioredoxin (right) responses.

Figure 6 - *In vivo* potential of DAC-paracetamol combination.

A-B. DAC-paracetamol synergy assessed in FaDu cells (as in Fig 1E-G); cell viability after treatment with fixed Cmax titrations of drugs (**A**) resulting in combination index (CI) shown in (**B**). CI value less than 1 denotes synergy.

C. Tumour growth of FaDu cells engrafted into NSG mice (Day 1, red arrow) treated as

indicated (black arrows).

D. Days to reach tumour size of 200 mm^3. Tumours below 200 mm^3 at the end of the experiment are counted as Day 25.

E. Tumour size at Day 15 and at the end of the study.

F. qRT-PCR for *PTGS2* and *CYP2E1* expression in tumour tissue.

G. qRT-PCR for *TP63* and *KRT5* expression in tumour tissue.

Data information: In A-B n=3. Mice groups: Ctrl (n=6), paracetamol (n=6), DAC (n=5), DAC+paracetamol (n=6). In D-G: a non-matched One-Way ANOVA with Dunnett's correction was used to compare treatments with control. To compare DAC and DAC+Para an unpaired two-tailed *t* test was used. Values are displayed as means ± SEM. Only significant p values are shown.

Figure. 7 - Potential of DAC-paracetamol combined treatment in AML.

A-C. DAC-paracetamol synergy determined in AML cell lines. Cell viability of SKM-1 (**A**) and HL-60 (**B**) treated as indicated for 72h. Combination index (CI) shown in (**C**).

D. Long term effects of DAC and DAC-paracetamol combined treatment on growth rates in SKM-1 (left) and HL-60 (right) cells: 4 cycles (C1-C4, 72h treatment as indicated followed by 21 day withdrawal). Vehicle and paracetamol controls are shown for the first 10 days.

E. qRT-PCR for *PTGS2*, *PTGER1*, *PTGER2* and *PTGER3* genes in SKM-1 and HL-60 cells after indicated treatments and shown relative to control.

F. qRT-PCR for *PTGS2* shown as in (E).

G. Levels of intracellular ROS measured by DCFDA staining and FACS in SKM-1 cells treated with indicated drugs and their combinations. Vald, 10 µM valdecoxib.

H. Levels of mitochondrial superoxide assessed by MitoSOX Red staining and FACS in SKM-1 cells as in (G).

I. Proportion of SKM-1 cells undergoing cell death assessed by FACS following Annexin V and PI staining.

J. Cell cycle distribution of SKM-1 cells after of DAC, paracetamol or combined treatment.

K. qRT-PCR for *CD11b* gene in SKM-1 and HL-60 cells after indicated treatments.

L. Giemsa-Jenner staining in SKM-1 cells. Upper: 100x magnification; lower: image zoomed to approximately one cell. Vacuole formation in cytoplasm indicated by black arrow.

Data information: Unless stated otherwise all treatments were for 72h with 500 nM DAC and 132.2 µM paracetamol and n=3. In E-H and K: a matched One-Way ANOVA with Dunnett's correction was applied to compare treatments with control; in G-H a separate ANOVA was

used to compare DAC to DAC+Para and DAC+Vald. In I-J: for each group a matched Two-Way ANOVA with Dunnett's was performed to compare treatments with control; a separate Two-Way ANOVA with Sidak's was used to compare DAC with DAC+Para. Values are displayed as means ± SEM. Only significant p values are shown.

References

Abele R, Clavel M, Dodion P, Bruntsch U, Gundersen S, Smyth J, Renard J, van Glabbeke M, Pinedo HM (1987) The EORTC Early Clinical Trials Cooperative Group experience with 5-aza-2'-deoxycytidine (NSC 127716) in patients with colo-rectal, head and neck, renal carcinomas and malignant melanomas. *Eur J Cancer Clin Oncol* 23: 1921-1924

Ashburner M, Ball CA, Blake JA, Botstein D, Butler H, Cherry JM, Davis AP, Dolinski K, Dwight SS, Eppig JT *et al* (2000) Gene ontology: tool for the unification of biology. The Gene Ontology Consortium. *Nat Genet* 25: 25-29

Bertolini A, Ferrari A, Ottani A, Guerzoni S, Tacchi R, Leone S (2006) Paracetamol: new vistas of an old drug. *CNS Drug Rev* 12: 250-275

Brown T (2001) Dot and slot blotting of DNA. *Curr Protoc Mol Biol* Chapter 2: Unit2 9B

Bryant J, Batis N, Franke AC, Clancey G, Hartley M, Ryan G, Brooks J, Southam AD, Barnes N, Parish J *et al* (2019) Repurposed quinacrine synergizes with cisplatin, reducing the effective dose required for treatment of head and neck squamous cell carcinoma. *Oncotarget* 10: 5229-5244

Cancer Genome Atlas N (2015) Comprehensive genomic characterization of head and neck squamous cell carcinomas. *Nature* 517: 576-582

Cebola I, Custodio J, Munoz M, Diez-Villanueva A, Pare L, Prieto P, Ausso S, Coll-Mulet L, Bosca L, Moreno V *et al* (2015) Epigenetics override pro-inflammatory PTGS transcriptomic signature towards selective hyperactivation of PGE2 in colorectal cancer. *Clin Epigenetics* 7: 74

Cebola I, Peinado MA (2012) Epigenetic deregulation of the COX pathway in cancer. *Prog Lipid Res* 51: 301-313

Chiappinelli KB, Strissel PL, Desrichard A, Li H, Henke C, Akman B, Hein A, Rote NS, Cope LM, Snyder A *et al* (2015) Inhibiting DNA Methylation Causes an Interferon Response in Cancer via dsRNA Including Endogenous Retroviruses. *Cell* 162: 974-986

Chou TC (2006) Theoretical basis, experimental design, and computerized simulation of synergism and antagonism in drug combination studies. *Pharmacol Rev* 58: 621-681

Dahlin DC, Miwa GT, Lu AY, Nelson SD (1984) N-acetyl-p-benzoquinone imine: a cytochrome P-450-mediated oxidation product of acetaminophen. *Proc Natl Acad Sci U S A* 81: 1327-1331

European Medicines Agency E, 2019. Dacogen, in: Agency E.M. (Ed.). https://www.ema.europa.eu/en/documents/product-information/dacogen-epar-product-information_en.pdf.

Forman HJ, Zhang H, Rinna A (2009) Glutathione: overview of its protective roles, measurement, and biosynthesis. *Mol Aspects Med* 30: 1-12

Gao J, Aksoy BA, Dogrusoz U, Dresdner G, Gross B, Sumer SO, Sun Y, Jacobsen A, Sinha R, Larsson E *et al* (2013) Integrative analysis of complex cancer genomics and clinical profiles using the cBioPortal. *Sci Signal* 6: pl1

Graham GG, Davies MJ, Day RO, Mohamudally A, Scott KF (2013) The modern pharmacology of paracetamol: therapeutic actions, mechanism of action, metabolism, toxicity and recent pharmacological findings. *Inflammopharmacology* 21: 201-232

Hedberg ML, Peyser ND, Bauman JE, Gooding WE, Li H, Bhola NE, Zhu TR, Zeng Y, Brand TM, Kim MO *et al* (2019) Use of nonsteroidal anti-inflammatory drugs predicts improved patient survival for PIK3CA-altered head and neck cancer. *J Exp Med* 216: 419-427

Jones PA, Baylin SB (2002) The fundamental role of epigenetic events in cancer. *Nat Rev Genet* 3: 415-428

Kantarjian HM, Thomas XG, Dmoszynska A, Wierzbowska A, Mazur G, Mayer J, Gau JP, Chou WC, Buckstein R, Cermak J *et al* (2012) Multicenter, randomized, open-label, phase III trial of decitabine versus patient choice, with physician advice, of either supportive care or low-dose cytarabine for the treatment of older patients with newly diagnosed acute myeloid leukemia. *J Clin Oncol* 30: 2670-2677

Khanim FL, Merrick BA, Giles HV, Jankute M, Jackson JB, Giles LJ, Birtwistle J, Bunce CM, Drayson MT (2011) Redeployment-based drug screening identifies the anti-helminthic niclosamide as anti-myeloma therapy that also reduces free light chain production. *Blood Cancer J* 1: e39

Kim YY, Lee EJ, Kim YK, Kim SM, Park JY, Myoung H, Kim MJ (2010) Anti-cancer effects of celecoxib in head and neck carcinoma. *Mol Cells* 29: 185-194

Kobrinsky NL, Hartfield D, Horner H, Maksymiuk A, Minuk GY, White DF, Feldstein TJ (1996) Treatment of advanced malignancies with high-dose acetaminophen and N-acetylcysteine rescue. *Cancer Invest* 14: 202-210

Kurtova AV, Xiao J, Mo Q, Pazhanisamy S, Krasnow R, Lerner SP, Chen F, Roh TT, Lay E, Ho PL *et al* (2015) Blocking PGE2-induced tumour repopulation abrogates bladder cancer chemoresistance. *Nature* 517: 209-213

Lamb J, Crawford ED, Peck D, Modell JW, Blat IC, Wrobel MJ, Lerner J, Brunet JP, Subramanian A, Ross KN *et al* (2006) The Connectivity Map: using gene-expression signatures to connect small molecules, genes, and disease. *Science* 313: 1929-1935

Linnekamp JF, Butter R, Spijker R, Medema JP, van Laarhoven HWM (2017) Clinical and biological effects of demethylating agents on solid tumours - A systematic review. *Cancer Treat Rev* 54: 10-23

Liu B, Qu L, Yan S (2015) Cyclooxygenase-2 promotes tumor growth and suppresses tumor immunity. *Cancer Cell Int* 15: 106

Napolitano F, Sirci F, Carrella D, di Bernardo D (2016) Drug-set enrichment analysis: a novel tool to investigate drug mode of action. *Bioinformatics* 32: 235-241

Nieto M, Demolis P, Behanzin E, Moreau A, Hudson I, Flores B, Stemplewski H, Salmonson T, Gisselbrecht C, Bowen D *et al* (2016) The European Medicines Agency Review of Decitabine (Dacogen) for the Treatment of Adult Patients With Acute Myeloid Leukemia:

Summary of the Scientific Assessment of the Committee for Medicinal Products for Human Use. *Oncologist* 21: 692-700

Park SW, Heo DS, Sung MW (2012) The shunting of arachidonic acid metabolism to 5-lipoxygenase and cytochrome p450 epoxygenase antagonizes the anti-cancer effect of cyclooxygenase-2 inhibition in head and neck cancer cells. *Cell Oncol (Dordr)* 35: 1-8

Posadas I, Vellecco V, Santos P, Prieto-Lloret J, Cena V (2007) Acetaminophen potentiates staurosporine-induced death in a human neuroblastoma cell line. *Br J Pharmacol* 150: 577-585

Qin T, Jelinek J, Si J, Shu J, Issa JP (2009) Mechanisms of resistance to 5-aza-2'-deoxycytidine in human cancer cell lines. *Blood* 113: 659-667

Raghunath A, Sundarraj K, Nagarajan R, Arfuso F, Bian J, Kumar AP, Sethi G, Perumal E (2018) Antioxidant response elements: Discovery, classes, regulation and potential applications. *Redox Biol* 17: 297-314

Ray PD, Huang BW, Tsuji Y (2012) Reactive oxygen species (ROS) homeostasis and redox regulation in cellular signaling. *Cell Signal* 24: 981-990

Roulois D, Loo Yau H, Singhania R, Wang Y, Danesh A, Shen SY, Han H, Liang G, Jones PA, Pugh TJ *et al* (2015) DNA-Demethylating Agents Target Colorectal Cancer Cells by Inducing Viral Mimicry by Endogenous Transcripts. *Cell* 162: 961-973

Saba NF, Choi M, Muller S, Shin HJ, Tighiouart M, Papadimitrakopoulou VA, El-Naggar AK, Khuri FR, Chen ZG, Shin DM (2009) Role of cyclooxygenase-2 in tumor progression and survival of head and neck squamous cell carcinoma. *Cancer Prev Res (Phila)* 2: 823-829

Simard EP, Torre LA, Jemal A (2014) International trends in head and neck cancer incidence rates: differences by country, sex and anatomic site. *Oral Oncol* 50: 387-403

Smirnov P, Safikhani Z, El-Hachem N, Wang D, She A, Olsen C, Freeman M, Selby H, Gendoo DM, Grossmann P *et al* (2016) PharmacoGx: an R package for analysis of large pharmacogenomic datasets. *Bioinformatics* 32: 1244-1246

Squier CA, Kremer MJ (2001) Biology of oral mucosa and esophagus. *J Natl Cancer Inst Monogr*: 7-15

Steinmann K, Sandner A, Schagdarsurengin U, Dammann RH (2009) Frequent promoter hypermethylation of tumor-related genes in head and neck squamous cell carcinoma. *Oncol Rep* 22: 1519-1526

Stresemann C, Lyko F (2008) Modes of action of the DNA methyltransferase inhibitors azacytidine and decitabine. *Int J Cancer* 123: 8-13

Supek F, Bosnjak M, Skunca N, Smuc T (2011) REVIGO summarizes and visualizes long lists of gene ontology terms. *PLoS One* 6: e21800

Telorack M, Meyer M, Ingold I, Conrad M, Bloch W, Werner S (2016) A Glutathione-Nrf2-Thioredoxin Cross-Talk Ensures Keratinocyte Survival and Efficient Wound Repair. *PLoS Genet* 12: e1005800

Traverso N, Ricciarelli R, Nitti M, Marengo B, Furfaro AL, Pronzato MA, Marinari UM, Domenicotti C (2013) Role of glutathione in cancer progression and chemoresistance. *Oxid Med Cell Longev* 2013: 972913

Tsai HC, Li H, Van Neste L, Cai Y, Robert C, Rassool FV, Shin JJ, Harbom KM, Beaty R, Pappou E *et al* (2012) Transient low doses of DNA-demethylating agents exert durable antitumor effects on hematological and epithelial tumor cells. *Cancer Cell* 21: 430-446

Wang D, Dubois RN (2010) Eicosanoids and cancer. *Nat Rev Cancer* 10: 181-193

Wu L, Shi W, Li X, Chang C, Xu F, He Q, Wu D, Su J, Zhou L, Song L *et al* (2016) High expression of the human equilibrative nucleoside transporter 1 gene predicts a good response to decitabine in patients with myelodysplastic syndrome. *J Transl Med* 14: 66

Wu YJ, Neuwelt AJ, Muldoon LL, Neuwelt EA (2013) Acetaminophen enhances cisplatin- and paclitaxel-mediated cytotoxicity to SKOV3 human ovarian carcinoma. *Anticancer Res* 33: 2391-2400

Yoh K, Prywes R (2015) Pathway Regulation of p63, a Director of Epithelial Cell Fate. *Front Endocrinol (Lausanne)* 6: 51

Figure 1

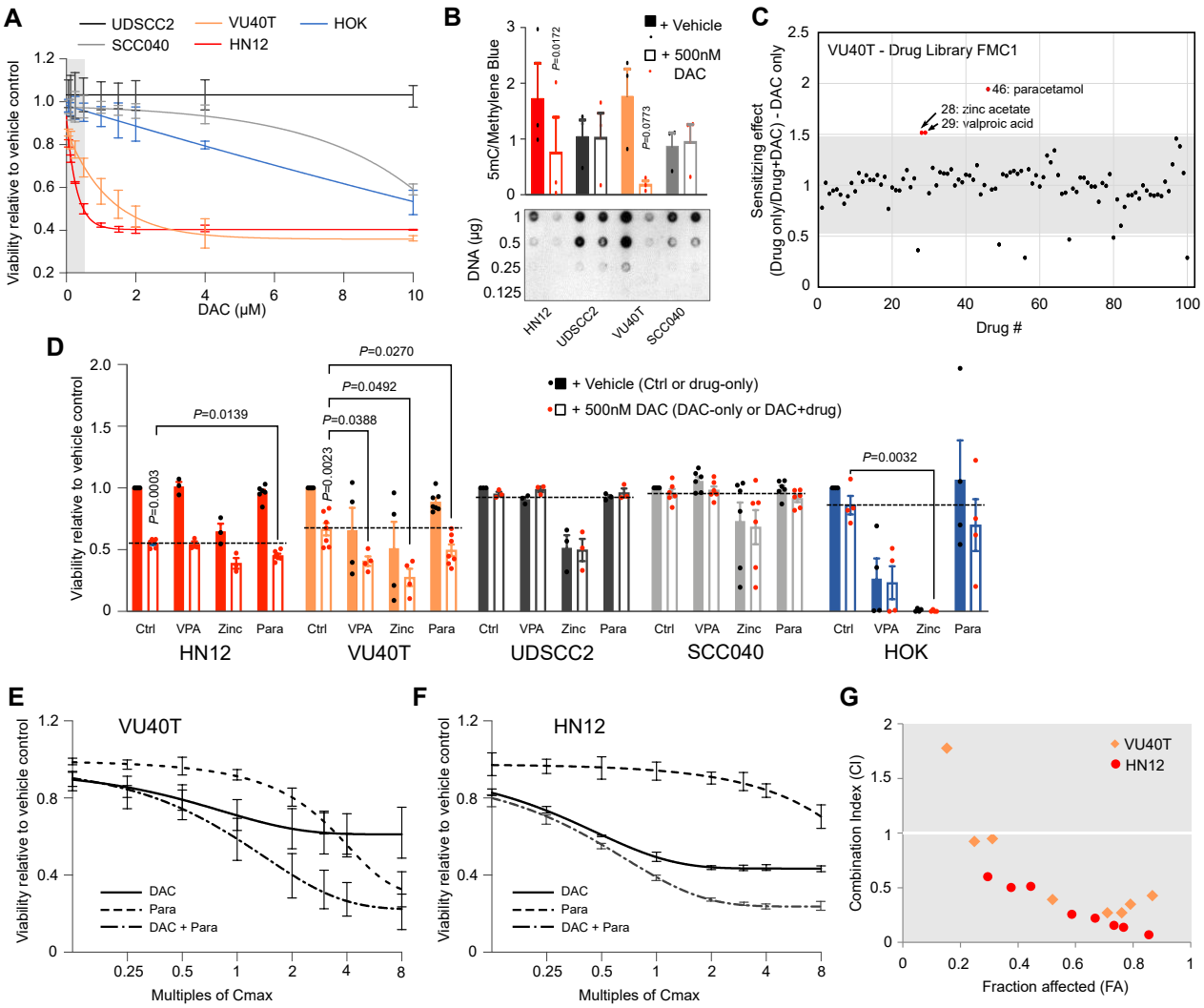
A
UDSCC2
SCC040
VU40T
HN12
HOK
Viability relative to vehicle control
DAC (μM)
B
+ Vehicle
+ 500nM DAC
5mC/Methylene Blue
P=0.0172
P=0.0773
DNA (μg)
HN12
UDSCC2
VU40T
SCC040
C
VU40T - Drug Library FMC1
46: paracetamol
28: zinc acetate
29: valproic acid
Sensitizing effect
(Drug only/Drug+DAC) - DAC only
Drug #
D
+ Vehicle (Ctrl or drug-only)
+ 500nM DAC (DAC-only or DAC+drug)
Viability relative to vehicle control
P=0.0139
P=0.0003
P=0.0388
P=0.0492
P=0.0023
P=0.0270
P=0.0032
Ctrl
VPA
Zinc
Para
HN12
VU40T
UDSCC2
SCC040
HOK

E
VU40T
Viability relative to vehicle control
DAC
Para
DAC + Para
Multiples of Cmax
F
HN12
Viability relative to vehicle control
DAC
Para
DAC + Para
Multiples of Cmax
G
VU40T
HN12
Combination Index (CI)
Fraction affected (FA)

Figure 2

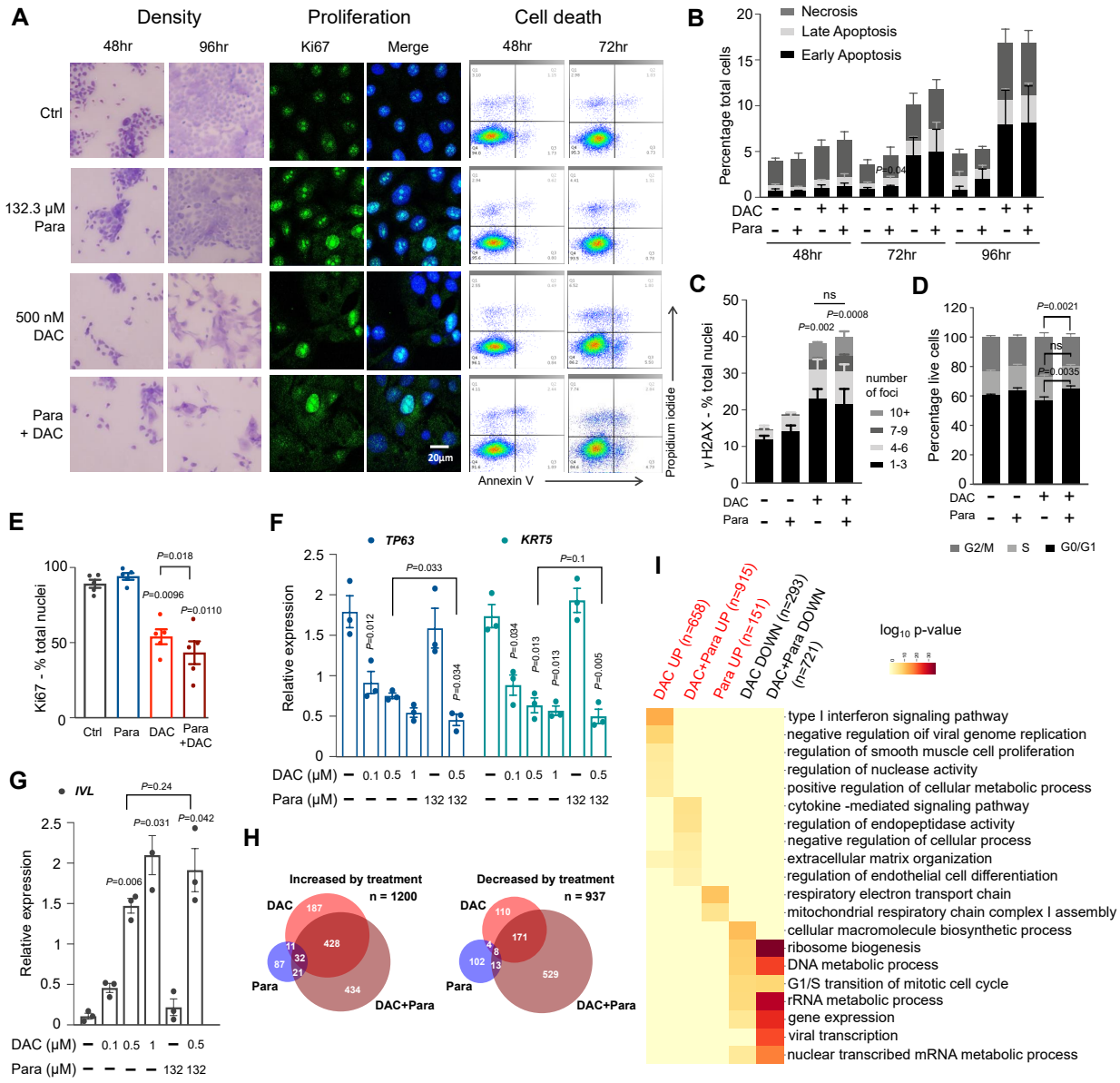
A
Density
Proliferation
Cell death
48hr
96hr
Ki67
Merge
48hr
72hr
Ctrl
132.3 μM Para
500 nM DAC
Para + DAC
20μm
Annexin V
Propidium iodide
B
Necrosis
Late Apoptosis
Early Apoptosis
Percentage total cells
P=0.04
DAC
Para
48hr
72hr
96hr
C
γ H2AX - % total nuclei
ns
P=0.0008
P=0.002
number of foci
10+
7-9
4-6
1-3
DAC
Para
D
Percentage live cells
P=0.0021
ns
P=0.0035
DAC
Para
G2/M
S
G0/G1
E
Ki67 - % total nuclei
P=0.018
P=0.0096
P=0.0110
Ctrl
Para
DAC
Para +DAC
F
TP63
KRT5
Relative expression
P=0.033
P=0.012
P=0.034
P=0.1
P=0.034
P=0.013
P=0.013
P=0.005
DAC (μM)
Para (μM)
G
IVL
Relative expression
P=0.24
P=0.031
P=0.042
P=0.006
DAC (μM)
Para (μM)
H
Increased by treatment
n = 1200
DAC
Para
DAC+Para
187
428
11
32
87
21
434
Decreased by treatment
n = 937
DAC
Para
DAC+Para
110
171
4
8
102
13
529
I
DAC UP (n=658)
DAC+Para UP (n=915)
Para UP (n=151)
DAC DOWN (n=293)
DAC+Para DOWN (n=721)
log10 p-value
type I interferon signaling pathway
negative regulation oif viral genome replication
regulation of smooth muscle cell proliferation
regulation of nuclease activity
positive regulation of cellular metabolic process
cytokine -mediated signaling pathway
regulation of endopeptidase activity
negative regulation of cellular process
extracellular matrix organization
regulation of endothelial cell differentiation
respiratory electron transport chain
mitochondrial respiratory chain complex I assembly
cellular macromolecule biosynthetic process
ribosome biogenesis
DNA metabolic process
G1/S transition of mitotic cell cycle
rRNA metabolic process
gene expression
viral transcription
nuclear transcribed mRNA metabolic process

Figure 3

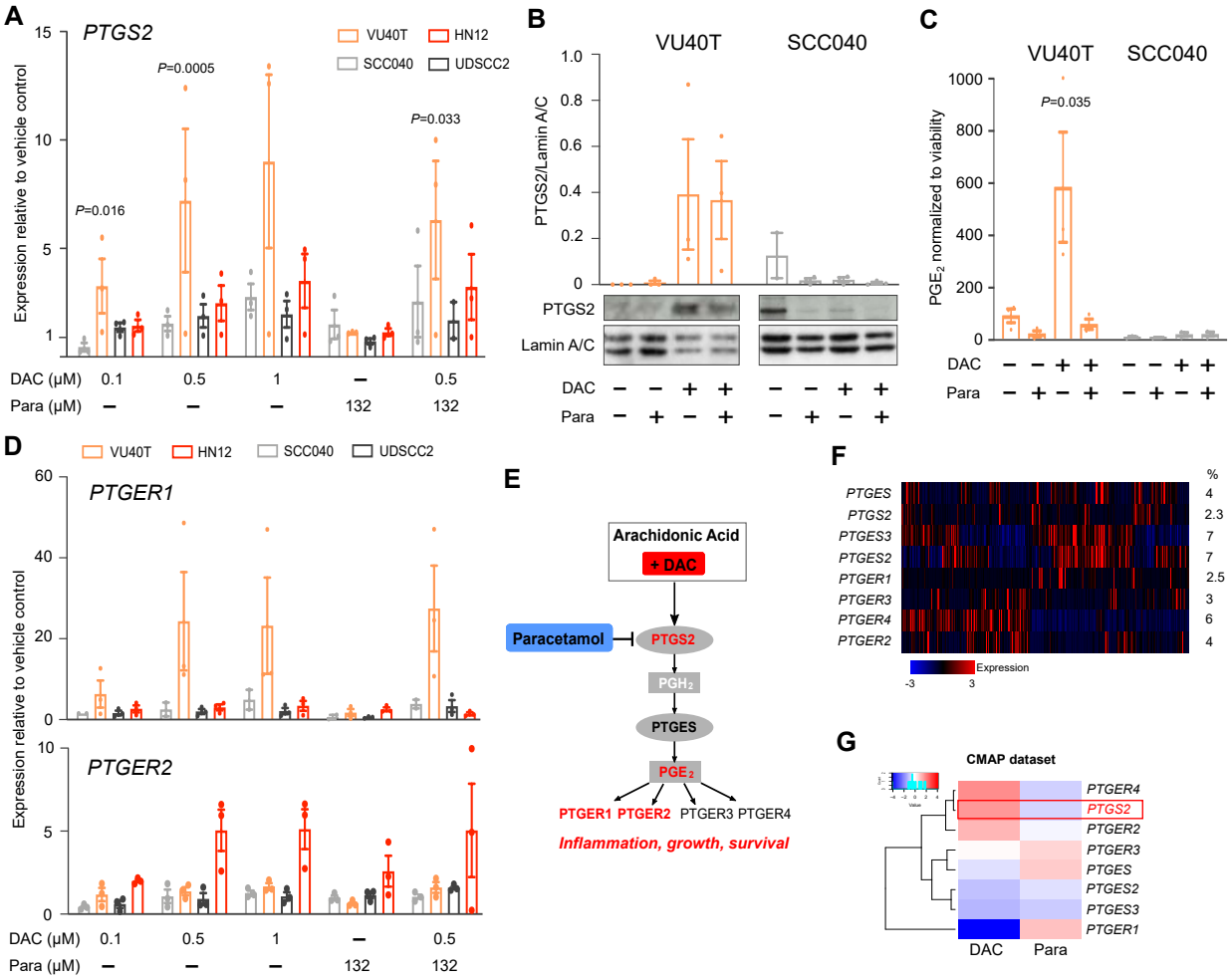
A
PTGS2
VU40T
HN12
SCC040
UDSCC2
P=0.0005
P=0.033
P=0.016
Expression relative to vehicle control
DAC (μM) 0.1 0.5 1 – 0.5
Para (μM) – – – 132 132
B
VU40T
SCC040
PTGS2/Lamin A/C
PTGS2
Lamin A/C
DAC – – + + – – + +
Para – + – + – + – +
C
VU40T
SCC040
P=0.035
PGE2 normalized to viability
DAC – – + + – – + +
Para – + – + – + – +
D
VU40T
HN12
SCC040
UDSCC2
PTGER1
PTGER2
Expression relative to vehicle control
DAC (μM) 0.1 0.5 1 – 0.5
Para (μM) – – – 132 132
E
Arachidonic Acid
+ DAC
Paracetamol
PTGS2
PGH2
PTGES
PGE2
PTGER1 PTGER2 PTGER3 PTGER4
Inflammation, growth, survival
F
%
PTGES 4
PTGS2 2.3
PTGES3 7
PTGES2 7
PTGER1 2.5
PTGER3 3
PTGER4 6
PTGER2 4
Expression
-3
3
G
CMAP dataset
PTGER4
PTGS2
PTGER2
PTGER3
PTGES
PTGES2
PTGES3
PTGER1
DAC
Para

Figure 4

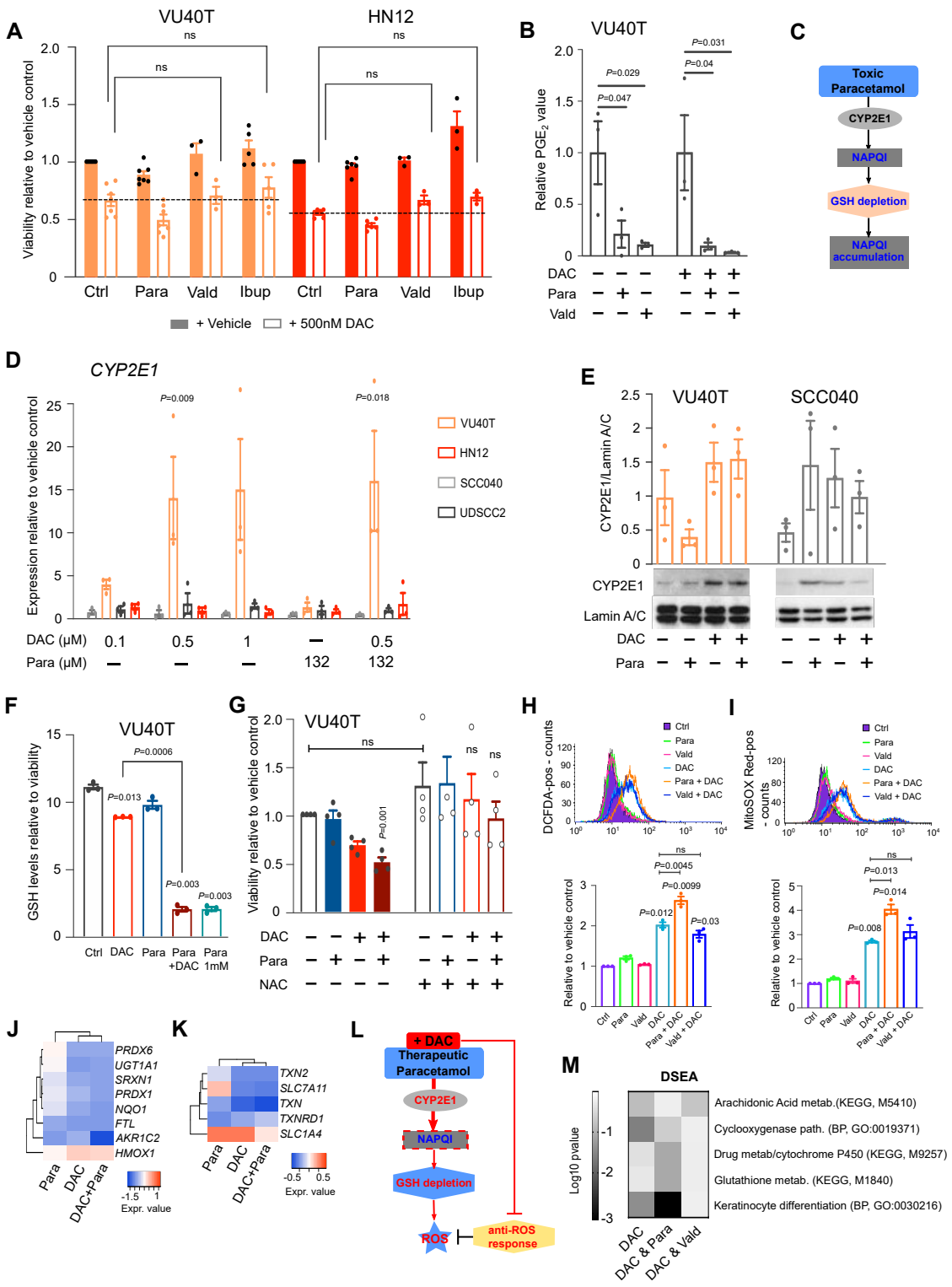
A
VU40T
HN12
ns
Viability relative to vehicle control
Ctrl
Para
Vald
Ibup
+ Vehicle
+ 500nM DAC
B
VU40T
Relative PGE2 value
P=0.029
P=0.047
P=0.031
P=0.04
DAC
Para
Vald
C
Toxic Paracetamol
CYP2E1
NAPQI
GSH depletion
NAPQI accumulation
D
CYP2E1
Expression relative to vehicle control
P=0.009
P=0.018
VU40T
HN12
SCC040
UDSCC2
DAC (μM)
Para (μM)
E
VU40T
SCC040
CYP2E1/Lamin A/C
CYP2E1
Lamin A/C
DAC
Para
F
VU40T
GSH levels relative to viability
P=0.0006
P=0.013
P=0.003
Ctrl
DAC
Para
Para +DAC
Para 1mM
G
VU40T
Viability relative to vehicle control
ns
P=0.001
DAC
Para
NAC
H
DCFDA-pos - counts
Ctrl
Para
Vald
DAC
Para + DAC
Vald + DAC
Relative to vehicle control
P=0.0045
P=0.0099
P=0.012
P=0.03
I
MitoSOX Red-pos - counts
P=0.013
P=0.014
P=0.008
J
PRDX6
UGT1A1
SRXN1
PRDX1
NQO1
FTL
AKR1C2
HMOX1
Para
DAC
DAC+Para
Expr. value
K
TXN2
SLC7A11
TXN
TXNRD1
SLC1A4
Para
DAC
DAC+Para
Expr. value
L
+ DAC
Therapeutic Paracetamol
CYP2E1
NAPQI
GSH depletion
ROS
anti-ROS response
M
DSEA
Log10 pvalue
Arachidonic Acid metab.(KEGG, M5410)
Cyclooxygenase path. (BP, GO:0019371)
Drug metab/cytochrome P450 (KEGG, M9257)
Glutathione metab. (KEGG, M1840)
Keratinocyte differentiation (BP, GO:0030216)
DAC
DAC & Para
DAC & Vald

Figure 5

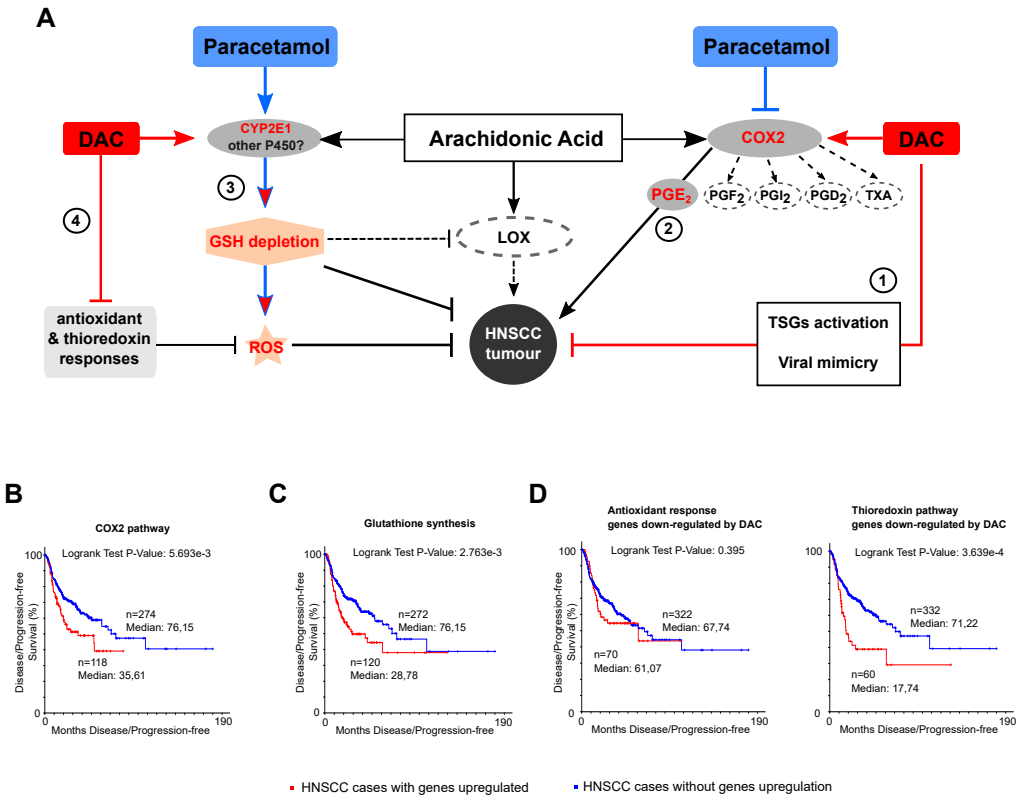
A
Paracetamol
Paracetamol
DAC
CYP2E1
other P450?
Arachidonic Acid
COX2
DAC
3
4
GSH depletion
LOX
PGE2
PGF2
PGI2
PGD2
TXA
2
1
antioxidant
& thioredoxin
responses
ROS
HNSCC
tumour
TSGs activation
Viral mimicry
B
COX2 pathway
Logrank Test P-Value: 5.693e-3
n=274
Median: 76,15
n=118
Median: 35,61
Disease/Progression-free Survival (%)
Months Disease/Progression-free
C
Glutathione synthesis
Logrank Test P-Value: 2.763e-3
n=272
Median: 76,15
n=120
Median: 28,78
D
Antioxidant response genes down-regulated by DAC
Logrank Test P-Value: 0.395
n=322
Median: 67,74
n=70
Median: 61,07
Thioredoxin pathway genes down-regulated by DAC
Logrank Test P-Value: 3.639e-4
n=332
Median: 71,22
n=60
Median: 17,74
HNSCC cases with genes upregulated
HNSCC cases without genes upregulation

Figure 6

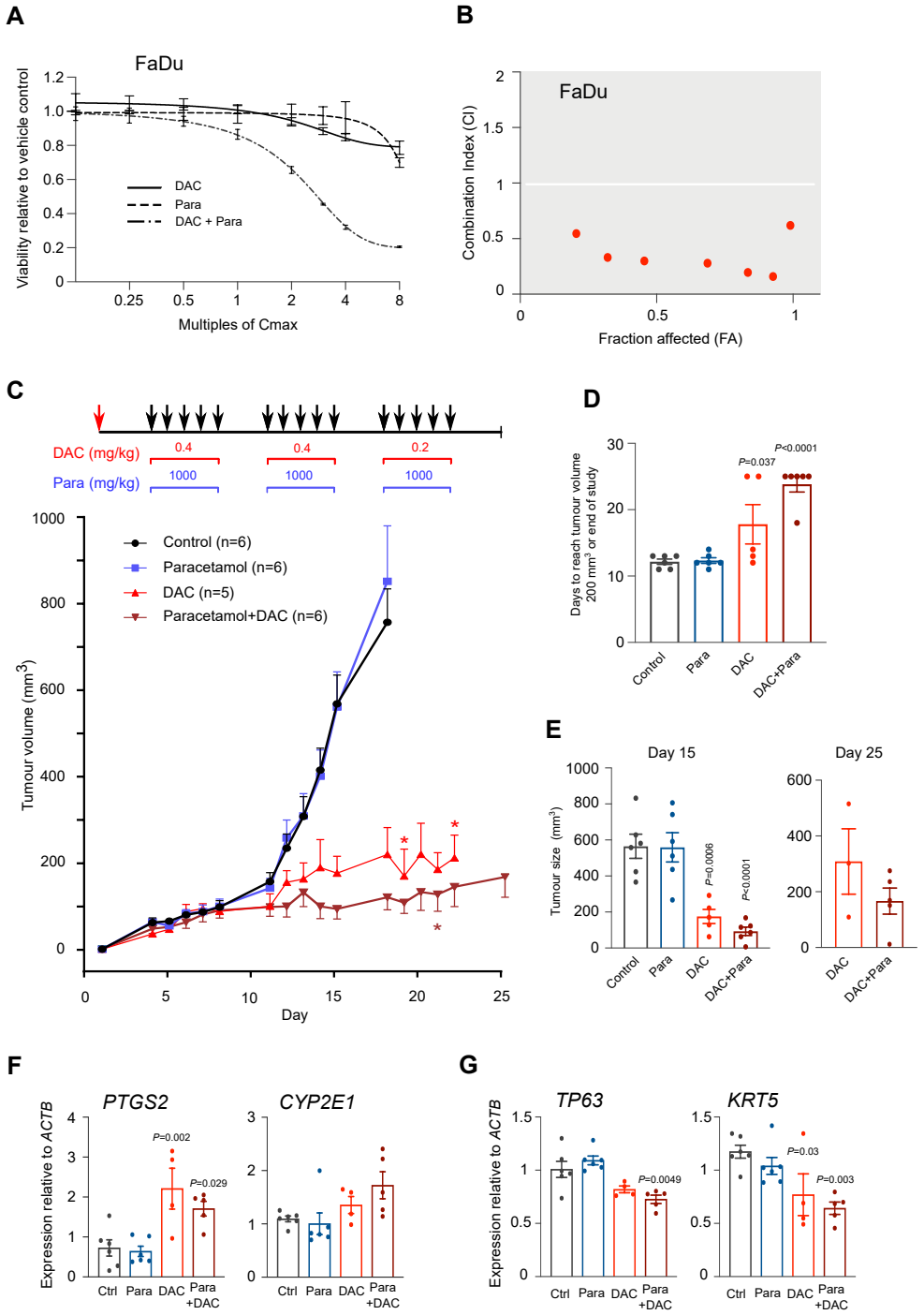
A
FaDu
Viability relative to vehicle control
DAC
Para
DAC + Para
Multiples of Cmax
B
FaDu
Combination Index (CI)
Fraction affected (FA)
C
DAC (mg/kg)
Para (mg/kg)
Control (n=6)
Paracetamol (n=6)
DAC (n=5)
Paracetamol+DAC (n=6)
Tumour volume (mm3)
Day
D
Days to reach tumour volume 200 mm3 or end of study
P=0.037
P<0.0001
Control
Para
DAC
DAC+Para
E
Day 15
Day 25
Tumour size (mm3)
P=0.0006
P<0.0001
F
PTGS2
CYP2E1
Expression relative to ACTB
P=0.002
P=0.029
Ctrl
Para
DAC
Para +DAC
G
TP63
KRT5
P=0.0049
P=0.03
P=0.003

Figure 7

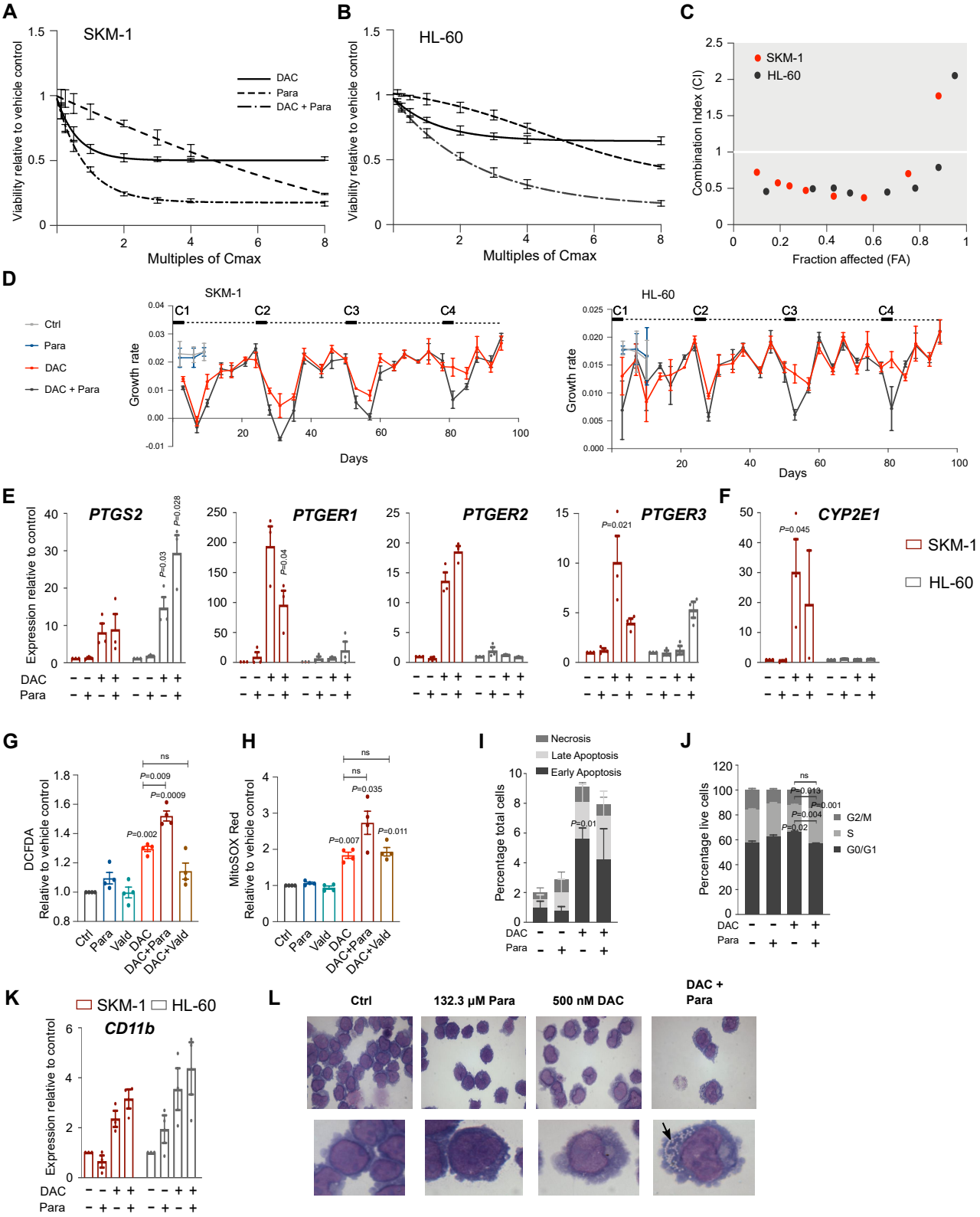
A
SKM-1
Viability relative to vehicle control
Multiples of Cmax
DAC
Para
DAC + Para
B
HL-60
Viability relative to vehicle control
Multiples of Cmax
C
SKM-1
HL-60
Combination Index (CI)
Fraction affected (FA)
D
SKM-1
HL-60
Ctrl
Para
DAC
DAC + Para
C1
C2
C3
C4
Growth rate
Days
E
PTGS2
PTGER1
PTGER2
PTGER3
Expression relative to control
P=0.028
P=0.03
P=0.04
P=0.021
F
CYP2E1
P=0.045
SKM-1
HL-60
DAC
Para
G
DCFDA
Relative to vehicle control
ns
P=0.009
P=0.0009
P=0.002
Ctrl
Para
Vald
DAC
DAC+Para
DAC+Vald
H
MitoSOX Red
Relative to vehicle control
ns
P=0.035
P=0.007
P=0.011
I
Necrosis
Late Apoptosis
Early Apoptosis
Percentage total cells
P=0.01
J
Percentage live cells
ns
P=0.013
P=0.001
P=0.004
P=0.02
G2/M
S
G0/G1
K
SKM-1
HL-60
CD11b
Expression relative to control
L
Ctrl
132.3 μM Para
500 nM DAC
DAC + Para

Supplementary information for:

A common analgesic enhances the anti-tumour activity of 5-aza-2'-deoxycytidine through induction of oxidative stress

Hannah J. Gleneadie, Amy Baker, Nikolaos Batis, Jennifer Bryant, Yao Jiang, Samuel J.H. Clokie, Hisham Mehanna, Paloma Garcia, Deena M.A. Gendoo, Sally Roberts, Alfredo A. Molinolo, J. Silvio Gutkind, Ben A. Scheven, Paul R. Cooper, Farhat L. Khanim, Malgorzata Wiench.

The Appendix contains the following supplementary information:

SI Materials and Methods

SI References

SI Tables S1 to S7

SI Figures S1 to S7

SI Materials and Methods

Detailed information is provided for the following methods and procedures: DNA dot blotting, Western blot analysis, immunofluorescence analysis, apoptosis assay, ROS and mitosox assessment, qRT-PCR, RNA-seq data analysis, mouse xenograft study, AML cells' growth rate assessment, TCGA data analysis and drug perturbation signatures.

Dot blotting of DNA

DNA was extracted using the DNeasy Blood and Tissue Kit (Qiagen) as described by the manufacturer. Dot blotting was performed as described in Current Protocols in Molecular Biology using a titration of DNA (Brown, 2001). Dried membranes (Nytran Supercharge Positively Charged Nylon Membrane (Fisher Scientific)) were blocked in 5% low-fat milk in PBS for 1h and incubated with primary antibody (anti-5mC, Cell Signalling (28692S), 1:750 dilution) in 1% bovine serum albumin (BSA) at 4°C overnight. Membranes were incubated with secondary antibody (Santa Cruz, Cat# sc-2004, 1:5000 dilution) for 2h at 4°C. Membranes were developed using 1:1 Amersham ECL western blotting reagent (GE Healthcare) to SuperSignal West Femto Chemiluminescent Substrate (Thermo Fisher Scientific) and detected by autoradiography. Blots were stained for total DNA by 30min incubation in 0.04% methylene blue (Sigma-Aldrich). ImageJ software (Schindelin *et al*, 2012) was used to quantify the intensity of the 1 μg and 0.5 μg dots and each 5-methylcytosine dot was normalised against its methylene blue counterpart. For each biological replicate an average was taken from the normalised 1 μg and 0.5 μg dots and the technical replicates for use in further analysis.

Western Blot analysis

Cell pellets were incubated with RIPA buffer (150mM sodium chloride, 0.5% sodium deoxycholate, 0.1% sodium dodecyl sulphate, 50mM Tris-HCl pH8) supplemented with protease inhibitors (Roche) for 45min then centrifuged at 17,000g for 10min and the supernatant was retained. Proteins were denatured in Laemmli buffer (4% SDS, 20% glycerol, 10% 2-mercaptoethanol, 0.004% bromophenol blue and 0.125 M Tris HCl), heated to 95°C for 5min and separated on a 10% SDS-PAGE gel before transferring onto a nitrocellulose membrane (Amersham Hybond ECL, GE Healthcare) using BioRad transfer apparatus. The protein transfer was confirmed with Ponceau S staining (SigmaAldrich).

Membranes were blocked in 20% milk in PBST for 1h following primary antibody incubation (COX-2: Abcam, Cat# ab15191, 1:1000 dilution, 1h at room temperature in 1%

BSA; CYP2E1: Abcam, Cat# ab28146, 1:2500 dilution, overnight 4°C in 5% milk; lamin A/C: Santa Cruz, Cat# sc-20681, 1:10,000, 1h at room temperature in 5% milk). Membranes were incubated with secondary antibody (anti-rabbit-IgG-HRP Santa Cruz, Cat# sc-2004, 1:5000 dilution) for 2h and developed as described for DNA dot blotting. ImageJ software was used to quantify the intensity of each band and bands of interest were normalised against the corresponding lamin A/C bands.

Immunofluorescence analysis

Immunofluorescence analysis was undertaken as described in (Roulois *et al*, 2015). For γH2AX staining, cells were first incubated with ice-cold pre-extraction buffer (10 mM PIPES pH 6.8, 300 mM sucrose, 20 mM NaCl, 3 mM $MgCl_2$ 0.5% Triton X-100) for 7min. For both γH2AX and Ki67 staining the cells were fixed in methanol for 15min, followed by 1min incubation with ice-cold acetate. Samples were blocked with 1% BSA in PBS for 1h at 4°C following incubation with the primary antibodies overnight (Ki67 (Abcam, Cat# ab15580) 1:1000; γH2AX (phospho S139) (Abcam, Cat# ab2893) 1:1000). Coverslips were incubated with secondary antibody (Jackson ImmunoResearch, Donkey anti-rabbit Alexa Fluor 488 cat# 711-545-152, 1:250) for 1h at room temperature, washed with PBS before drying and mounting using ProLong Gold Antifade Mountant with DAPI (Fisher Scientific). Cells were stored in the dark for 3 days prior to imaging on a Zeiss 780 Zen confocal microscope. For Ki67 staining, ImageJ was used to count percentage of positive cells in triplicate images from each biological replicate. For γH2AX staining, the number of γH2AX per nuclei was counted manually across all focal planes. 100 nuclei were analysed in each biological replicate.

Apoptosis assay

Following flow cytometry for cells stained with annexin V and propidium iodide (PI), the cells were gated into four populations and counted: healthy cells which were positive for neither PI nor annexin V; necrotic cells stained only with PI; early apoptotic cells stained only with annexin V and late apoptotic cells stained with both PI and annexin V. The proportion of cells in each quadrant after 48h, 72h, 96h of treatment was counted and compared to the vehicle control.

Assessment of reactive oxygen species (ROS) and mitochondrial superoxide (mitosox)

MitoSOX Red (Molecular Probes, Cat# M36008, ThermoFisher Scientific) was used to assess mitosox. PBS-washed cells were resuspended in 200 µl PBS (37°C) containing 5 µM

MitoSOX Red, incubated at 37°C for 10 min and then analysed by flow cytometry (emission wavelength 580 nm). Reactive oxygen species (ROS) were measured using carboxy-H_2DCFDA (5-(and-6)-carboxy-2',7'-dichlorodihydrofluorescein diacetate, Cat# C369, Invitrogen). 10 µM carboxy-H_2DCFDA was added to 0.5 ml cell suspension for 45 min, cells were washed with PBS and resuspended in 200 µl PBS (37°C). Resuspended cells were analysed by flow cytometry (emission wavelength 517-527 nm) with BD FACSCalibur and BD Cell Quest software. The geometric mean was calculated for each sample and experimental condition.

Real-Time quantitative PCR (qRT-PCR)

The primers used in qRT-PCR are listed in Appendix Table S7. Relative RNA values were normalised against the concentration of the purified cDNA as measured by Qubit dsDNA High Sensitivity Assay kit (Thermo Fisher Scientific). This method of normalization was treated as an additional step to the normalization to *ACTB* expression because the DAC treatments can lead to decrease of RNA yield and changes in housekeeping gene expression. Each sample was examined at least in triplicate. PCR product specificity was confirmed by a melting-curve analysis.

RNA sequencing

Quantification of the RNA sequencing data was performed according to the latest recommended pipeline as defined in the DeSeq2 software. A count for each gene was calculated using the reference-free aligner Salmon (Patro *et al*, 2017) and the resulting count table was processed using DeSeq2 (Love *et al*, 2014) to compare treatment groups. There were 1200 upregulated (log2 fold change ≥1) and 937 downregulated (log2 fold change ≤-1) genes, further divided into six groups: i) genes up-regulated by paracetamol (n=151); ii) genes down-regulated by paracetamol (n=127); iii) genes up-regulated by DAC (n=658); iv) genes down-regulated by DAC (n=293); v) genes up-regulated by combined treatment (n=915); and vi) genes down-regulated by combined treatment (n=721). Each group was subjected to gene ontology (GO) analysis using the Gene Ontology Consortium software (Ashburner *et al*, 2000) followed by removal of redundant terms using REVIGO (Supek *et al*, 2011). The top 5 terms with the Log_{10} p-value ≤3.0 from each group were collated; none of the GO terms from the gene set downregulated by paracetamol fulfilled this condition. The Log_{10} p-values were used to generate heatmap.

Mouse xenograft study – detailed protocol

To examine the toxicity and anti-tumour efficacy of DAC and paracetamol, we utilised male NOD/SCID/gamma (NSG) mice (Charles River) which were kept in 12 hour light and 12 hour dark cycles in individually ventilated cages. Mice were maintained on mouse feed and water, ad libitum, and were at least 6 weeks old at the start of the treatments.

Toxicity studies with 3 animals per single treatment and combination treatment were used to identify safe doses for use in subsequent efficacy study: 0.4 mg/kg DAC and 1000 mg/kg paracetamol. In the toxicity studies the drugs were given 5 days a week for three weeks, first for DAC and paracetamol separately and then in combination.

To assess the efficacy, 24 male NSG mice were implanted with $5x10^6$ FaDu HNSCC cells suspended in serum-free medium and injected subcutaneously into the right flank. Tumours were given three days to become established, at which point mice were randomly allocated into four treatment groups, each group containing 6 animals, as follows: (1) 0.4 mg/kg DAC dissolved in PBS via intraperitoneal (IP) injection on a 5 day on, 2 day off regimen from day 4 onwards; (2) 1000 mg/kg paracetamol dissolved in PBS given via oral gavage following the same regimen; (3) DAC plus paracetamol as above; (4) control (PBS) given both through the oral gavage and IP injection. Animals were monitored daily for signs of ill health and the tumours were measured. Tumour measurements were taken using callipers and volumes calculated using the formula $L \times W^2$. Mice were culled once tumours reached a maximum of 1250 mm^3; tumours became ulcerated; when animals showed signs of ill health; or at the completion of the study. One mouse from group 1 had to be excluded on Day 10 due to dosing error. When displaying tumour growth over time, to gain an understanding of efficacy over a longer period of time, data were plotted until at least 4 animals per group remained; when fewer animals remained in a group, no more data were plotted. The tumour growth is also shown as time to reach volume of 200 mm^3; tumours smaller than 200 mm^3 at the end of the study (day 25) were counted as 'Day 25'. The difference in tumour size for each group was shown at day 15 (Control n=6, paracetamol n=6, DAC n=5, DAC+paracetamol n=6) and at the end of the study (day 25: DAC n=3 and DAC+paracetamol n=5).

Tumours were excised and snap frozen for subsequent analysis. Tumour tissue was available from 6 animals in control and paracetamol-treated groups, 4 animals from DAC-treated and 5 animals from DAC+paracetamol treated groups. Approximately 10-20mg tissue was pulverized and total RNA extracted as described before (see: Real-time quantitative PCR).

Long treatment of AML cells and growth rate assessment

SKM-1 and HL-60 cells were subjected to a repeated cycle of treatments. The cells were plated in 6-well plates at $0.5x10^6$ cells/ml and $0.375x10^6$ cells/ml for SKM-1 and HL-60, respectively, treated for 72h after which the cells were counted and re-plated without drugs at original concentrations. The withdrawal period lasted 21 days during which the cells were passaged twice a week. The treatment cycle was repeated four times and the cells were counted at each passage using trypan blue (Sigma-Aldrich) staining and haemocytometer cell counting. Growth rate was calculated using the following equation Gr=ln(N(t)/N(0))/t, where Gr = growth rate, N(t)=number of cells at time t, N(0)=number of cells at time 0, and t=time(hours).

TCGA data

The following data were retrieved from The Cancer Genome Atlas (TCGA) via cBioPortal for Cancer Genomics (Cerami *et al*, 2012; Gao *et al*, 2013): (i) expression and genetic alterations in *TP63* gene available for 496 patients (Appendix Fig S2); (ii) percentage of samples for each cancer type with mRNA Expression z-score threshold ± 2.0 (RNA Seq V2 RSEM) for all cancers with available TCGA provisional data (Appendix Tables S5 and S6); (iii) clustered gene expression heatmap for genes in COX-2 pathway in HNSCC tumours (520 patients, Fig. 3F); (iv) Logrank test p-values for overall survival and/or disease/progression-free survival for all cancers with available TCGA provisional data in indicated set of genes (expression z-score threshold ± 2.0), (Appendix Tables S5 and S6, Fig. 5B-D, Appendix Fig. S6); (v) Kaplan-Meier curves for HNSCC (520 patients) disease-progression free survival based on gene expression alterations in indicated sets of genes. The following gene sets have been used: COX-2 pathway (*PTGS2*, *PTGES*, *PTGES2*, *PTGES3*, *PTGER1*, *PTGER2*, *PTGER3*, *PTGER4*; Fig. 5B); Glutathione synthesis (*GSS*, *GCLC*, *GCLM*, *GGCT*, *OPLAH*, *GSR*; Fig. 5C); Antioxidant response genes down-regulated by DAC (*PRDX1*, *PRDX6*, *SRXN1*, *UGT1A1*, *NQO1*, *FTL*, *AKR1C2*; Fig. 5D); Thioredoxin pathway genes down-regulated by DAC (*TXN2*, *SLC7A11*, *TXN*, *TXNRD1*; Fig. 5D); COX-2-PGF_2, -PGI_2, -PGD_2, -TBX_2 pathways (*PTGS2*, *PTGDR2*, *PRXL2B*, *PTGDS*, *PTGIS*, *PTGIR*, *PTGFR*, *TBXA2R*, *TBXAS1*; Appendix Fig. S6A); LOX pathway (*ALOX5*, *ALOX15*, *ALOX15B*, *ALOX12*, *LTA4H*; Appendix Fig. S6B).

Drug perturbation signatures

Drug perturbation signatures were downloaded for the BROAD Connectivity Map dataset (CMAP) using the PharmacoGx package (version 1.14.0) (Smirnov *et al*, 2016) in R. cMap drug perturbation signatures represent transcriptionally profiled, drugs-treated cancer cell

lines involving 11,833 genes and 1,309 drugs across 5 cancer cell lines (breast cancer MCF7 and ssMCF7, pancreatic cancer PC3, melanoma SKMEL5 and AML HL-60). Precomputed signatures for CMAP were available for 1288 drugs; the signatures are calculated using a linear regression model adjusted for treatment duration, cell line identity, and batch, as described previously (Smirnov *et al.*, 2016). Heatmaps of drug perturbation signatures (transcriptional profiles) for Decitabine (DAC), paracetamol (Para), and Valdecoxib were plotted using ggplots package (version 3.0.1.1). All analyses have been conducted using the R statistical software (version 3.6.0); listed software dependencies are available on the Comprehensive Repository R Archive Network (CRAN) or Bioconductor (BioC).

SI References

Ashburner M, Ball CA, Blake JA, Botstein D, Butler H, Cherry JM, Davis AP, Dolinski K, Dwight SS, Eppig JT *et al* (2000) Gene ontology: tool for the unification of biology. The Gene Ontology Consortium. *Nat Genet* 25: 25-29

Brown T (2001) Dot and slot blotting of DNA. *Curr Protoc Mol Biol* Chapter 2: Unit2 9B

Cerami E, Gao J, Dogrusoz U, Gross BE, Sumer SO, Aksoy BA, Jacobsen A, Byrne CJ, Heuer ML, Larsson E *et al* (2012) The cBio cancer genomics portal: an open platform for exploring multidimensional cancer genomics data. *Cancer Discov* 2: 401-404

Gao J, Aksoy BA, Dogrusoz U, Dresdner G, Gross B, Sumer SO, Sun Y, Jacobsen A, Sinha R, Larsson E *et al* (2013) Integrative analysis of complex cancer genomics and clinical profiles using the cBioPortal. *Sci Signal* 6: pl1

Love MI, Huber W, Anders S (2014) Moderated estimation of fold change and dispersion for RNA-seq data with DESeq2. *Genome Biol* 15: 550

Patro R, Duggal G, Love MI, Irizarry RA, Kingsford C (2017) Salmon provides fast and bias-aware quantification of transcript expression. *Nat Methods* 14: 417-419

Roulois D, Loo Yau H, Singhania R, Wang Y, Danesh A, Shen SY, Han H, Liang G, Jones PA, Pugh TJ *et al* (2015) DNA-Demethylating Agents Target Colorectal Cancer Cells by Inducing Viral Mimicry by Endogenous Transcripts. *Cell* 162: 961-973

Schindelin J, Arganda-Carreras I, Frise E, Kaynig V, Longair M, Pietzsch T, Preibisch S, Rueden C, Saalfeld S, Schmid B *et al* (2012) Fiji: an open-source platform for biological-image analysis. *Nat Methods* 9: 676-682

Smirnov P, Safikhani Z, El-Hachem N, Wang D, She A, Olsen C, Freeman M, Selby H, Gendoo DM, Grossmann P *et al* (2016) PharmacoGx: an R package for analysis of large pharmacogenomic datasets. *Bioinformatics* 32: 1244-1246

Supek F, Bosnjak M, Skunca N, Smuc T (2011) REVIGO summarizes and visualizes long lists of gene ontology terms. *PLoS One* 6: e21800

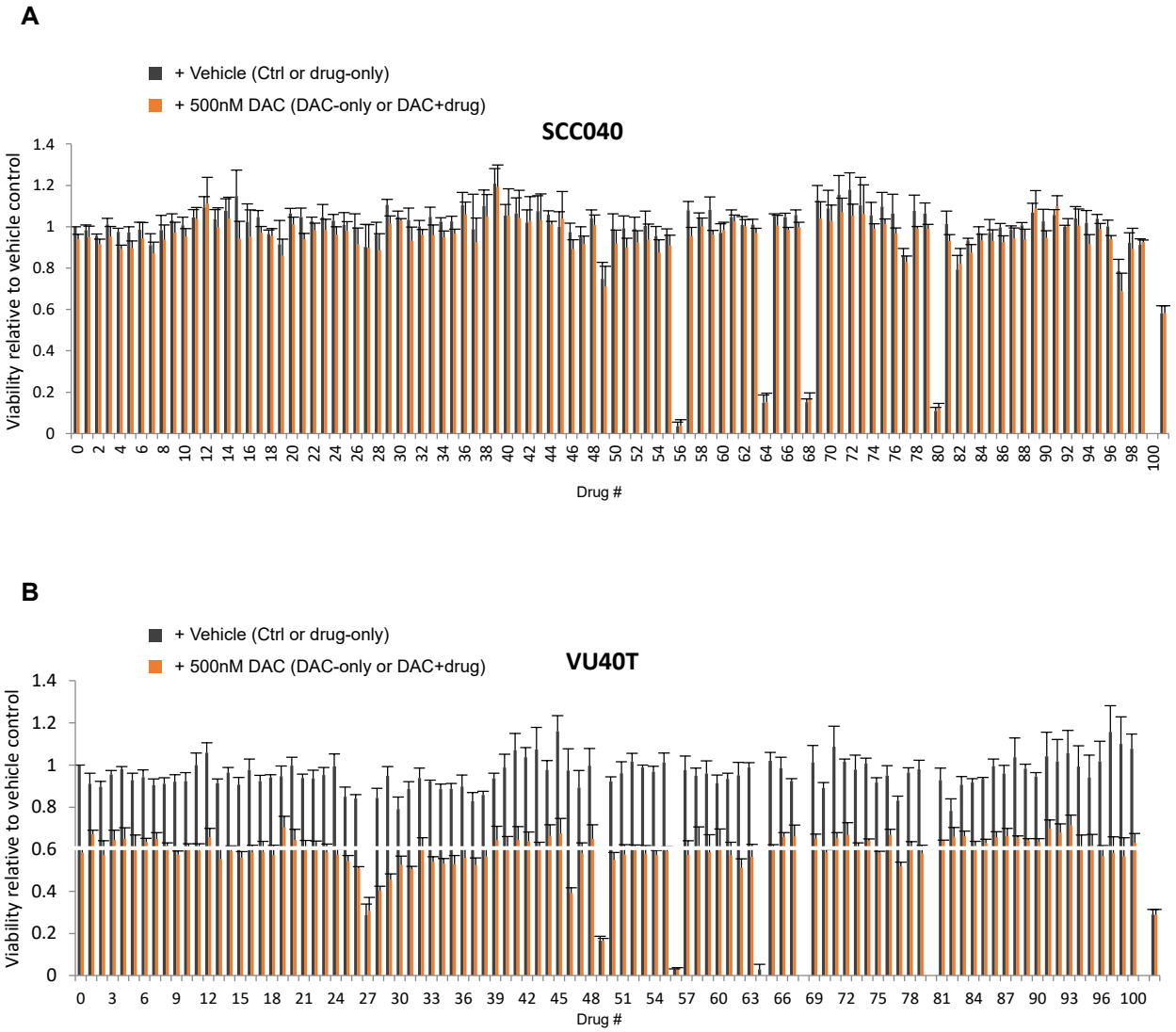

Figure S1. Sensitivity of HNSCC cells to DAC treatment can be increased by drug combinations.

A-B. DAC sensitizing assay: SCC040 (**A**) and VU40T (**B**) cells were subjected to 96h treatment with one of a panel of 100 drugs, +/-500 nM DAC. Viability was recorded and is shown here relative to the vehicle only control cells (Drug #0 black bar). The horizontal white line shows the effect of 500 nM DAC alone. The bars far right (Drug #101) show the effect of 10 µM DAC. The sensitizing effect is observed when the combined effect of the two drugs is more effective than both DAC alone and the drug alone. The assay was performed in triplicate and error bars represent SEM.
Drug #28: zinc acetate, #29: valproic acid, #46: paracetamol.

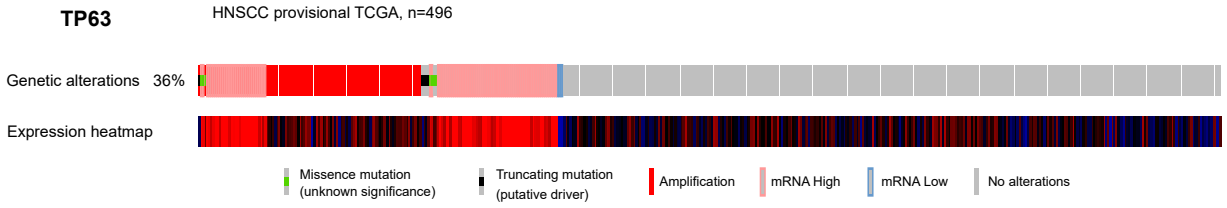

Figure S2 - *TP63* gene alterations in head and neck squamous cell carcinoma.
Genomic and expression alterations in *TP63* gene in 496 tumours from the provisional TCGA cohort of HNSCC patients. Upper graph shows genetic and expression (z-score => or =<2.0) alterations, explained in the legend; lower graph depicts expression heatmap.

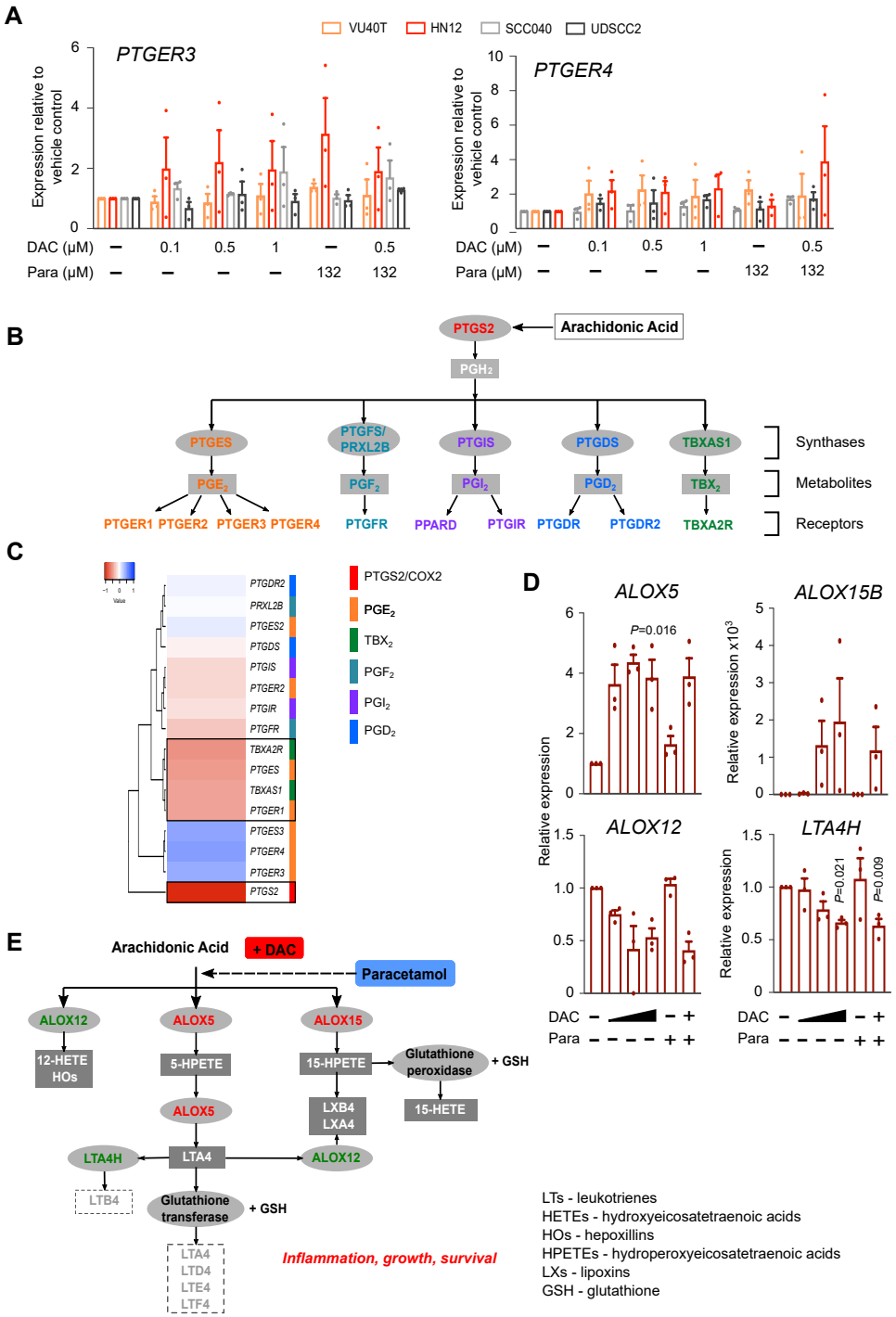

Figure S3 - COX-2 pathways are selectively affected by DAC treatment.

A. qRT-PCR for *PTGER3* and *PTGER4* genes in HNSCC cell lines treated for 96h with DAC and/or paracetamol as indicated. Data are shown as relative to vehicle control.

B. Schematic representation of the cyclooxygenase pathway. COX enzymes convert arachidonic acid (AA) into prostaglanding H_2 which is then converted to prostanoids (prostaglandins PGE_2, PGF_2, PGI_2, PGD_2 and thromboxane TXA_2) by respective synthases. Prostanoids are then recognized by G-protein coupled receptors in both autocrine and paracrine manner.

C. DAC-induced expression fold changes for genes encoding synthases and receptors involved in all cyclooxygenase pathways. Data obtained through RNA-seq in VU40T cells treated with 500 nM DAC for 96h. Black boxes indicate genes with highest upregulation. Colour-coded association with a specific pathway is shown to the right.

D. qRT-PCR for LOX pathway enzymes: *ALOX5*, *ALOX15B*, *ALOX12* and *LTA4H* in VU40T cells treated for 96h as indicated. Data are shown as relative to vehicle control.

E. Schematic of LOX pathway with confirmed DAC effects (up-regulation in red, down-regulation in green). Leukotrienes (LTs) shown in dotted boxes were below the detection levels of ELISA.

Data information: In A and D n=3, for each cell line a matched One-Way ANOVA with Dunnett's correction to compare all treatments to Ctrl. Values displayed as means +/-SEM. Only significant p-values are shown.

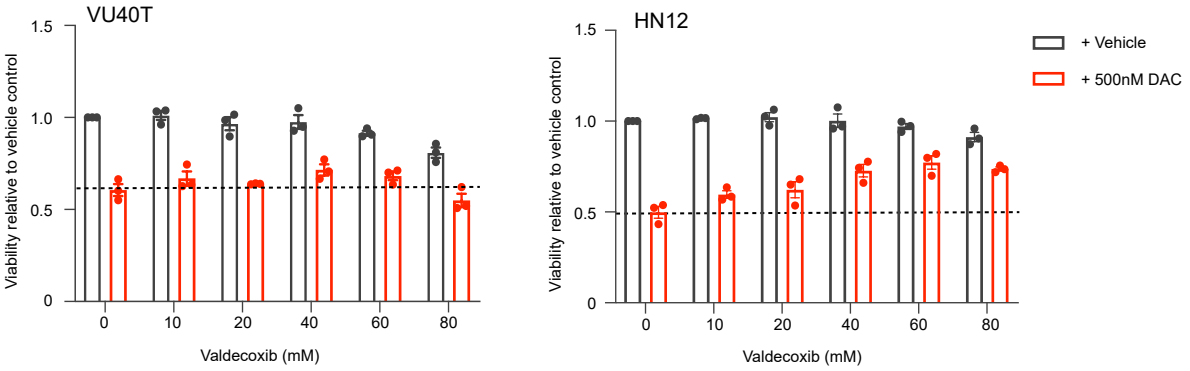

Figure S4. Valdecoxib does not sensitize HNSCC cells to DAC treatment.
VU40T and HN12 cell viability after 96h of treatment with indicated concentrations of Valdecoxib with or without 500 nM DAC. Dotted lines indicate viabillity at 500 nM DAC only. Mean ±SEM; n=3.

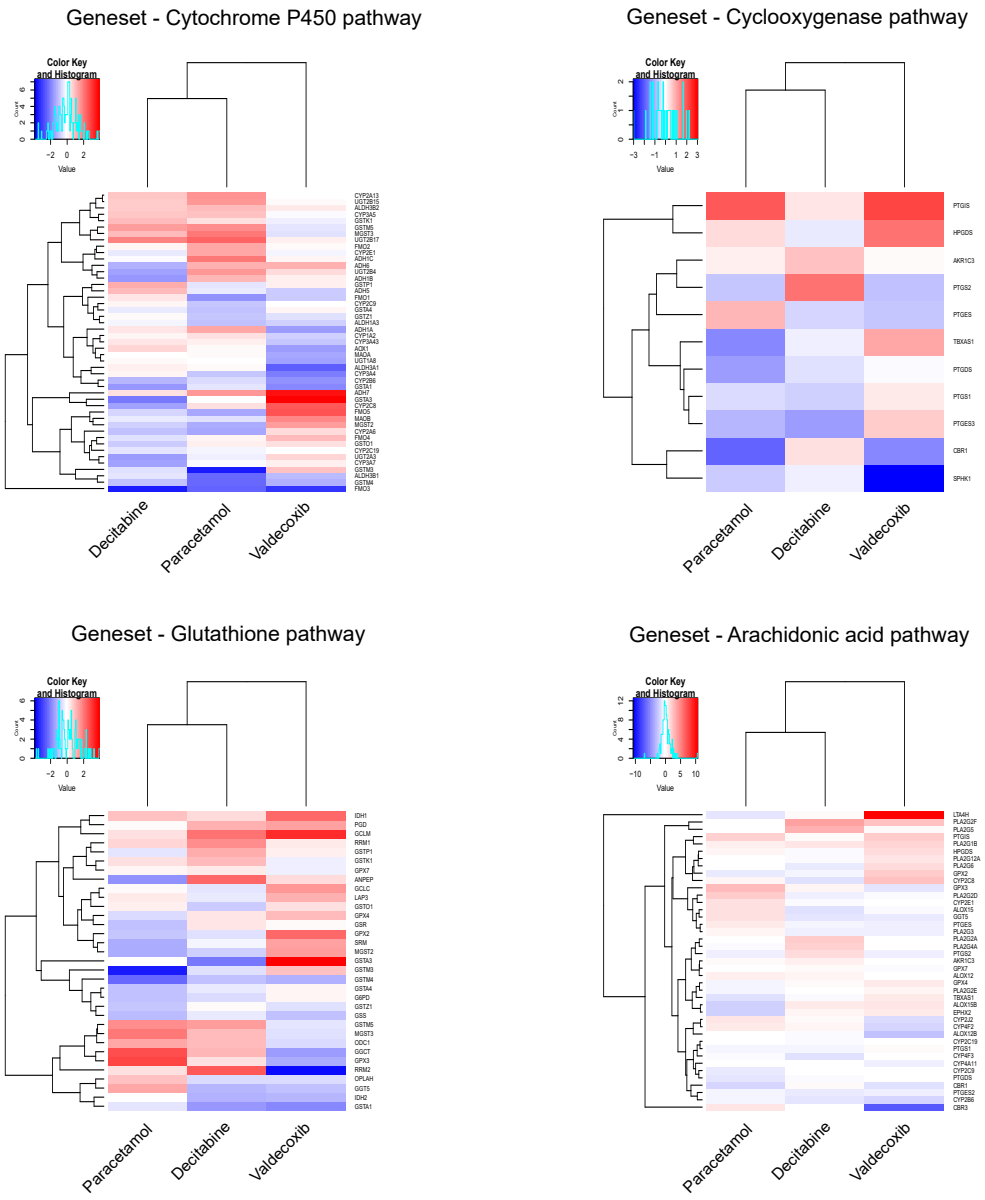

Figure S5 - DAC and paracetamol gene expression signatures share similar pathway enrichment. Drug perturbation signatures of Decitabine, paracetamol and valdecoxib, plotted for subsets of genes representing key pathways of interest that were identified from the DSEA analysis. Genes pertaining to each pathway were subsequently obtained from the corresponding genesets identified in MSigDB collection. Clustering of the drug perturbation profiles across these pathways indicates that Decitabine and paracetamol share similar drug perturbation profiles, compared to valdecoxib.

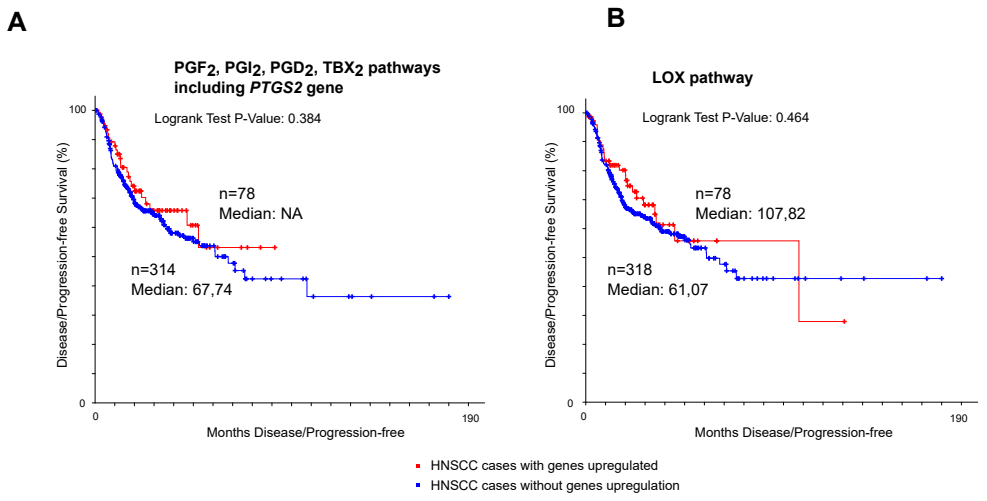

Figure S6 - COX-2 pathway alterations selectively affect HNSCC patients survival.

A. Disease/Progression-free survival curves for 392 HNSCC patients with data available in TCGA provisional cohort and gene upregulation for cyclooxygenase pathways other then PGE_2 (but including *PTGS2* gene).

B. Disease/Progression-free survival curves for 392 HNSCC patients with data available in TCGA provisional cohort and gene upregulation for LOX pathway.

Kaplan-Meier Estimates were obtained and plotted using cBioPortal.

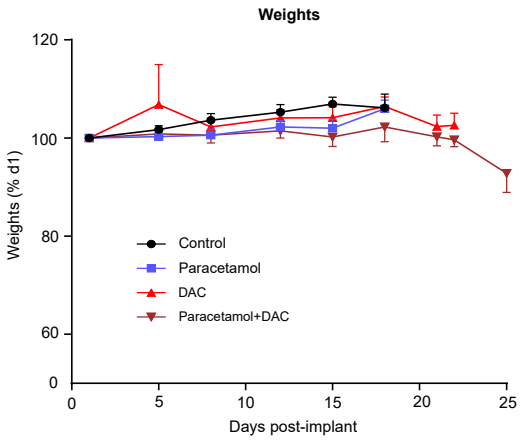

Figure S7 - *In vivo* potential of DAC-paracetamol combination.
Mice weights recorded during the efficacy study comparing treatments with DAC alone, paracetamol alone and DAC+paracetamol combination.

SI Supplementary Tables

Table S1. DRI (Dose Reduction Index) for VU40T, combined treatment.

Fa (%)	VU40T			
	Dose		DRI	
	DAC	Para	DAC	Para
10	0.01	105	0.30	10.18
25	0.16	251	1.22	7.11
50	2.26	595	**4.99**	**4.97**
75	31	1414	20.35	3.47
97	9300	9200	426	1.59

Table S2. DRI for HN12, combined treatment.

Fa (%)	HN12			
	Dose		DRI	
	DAC	Para	DAC	Para
10	0.004	186	0.49	80
25	0.06	1962	1.19	147
50	0.85	20653	**2.92**	**269**
75	11.92	217412	7.15	493
97	3630	3.55E+07	49.5	1827

Table S3. Differentially expressed genes in VU40T cells.

Increased by treatment			Decreased by treatment		
DAC	**Para**	**DAC+Para**	**DAC**	**Para**	**DAC+Para**
IFITM1	PTPRA	MT-ND1	STYXL1	FLOT1	MRPL15
OLR1	PHLPP1	MT-ND6	FAM172A	ZNF254	CDCA8
IFI6	INHBB	MT-ND4	ARHGEF10	AP002990.1	RRP8
LXN	TGM1	MT-ND5	MTO1	VAC14	TRAPPC5
PADI3	GPR37L1	TIMP3	PFAS	ALDH1A3	ADSL
FSTL1	GNL1	KLF15	PPIA	SBF1	ITPA
H1F0	SREK1	SERPINA1	TOX	HAUS5	RRP1
TNFSF10	MT-ATP6	MT-ATP6	PWP2	ASAH2	WIPF3
CLDN1	GPM6A	SLITRK6	MMP16	CCDC22	FLVCR1
STEAP4	ZNF302	SMARCA1	SBF1	PLD6	TMEM107
MTRNR2L1	BBS2	MUC16	EHMT2	TTC6	FABP5
GATA3	FGF23	GSN	RRM1	ERMAP	SLC7A5
FBLN1	NEGR1	OXTR	RPS21	ITPR1	CCNF
MMP13	HMGN5	CADM4	RPL22	AHNAK2	CA2
MUC20	GRAMD1C	MT-ATP8	RWDD2B	RABAC1	FAM57A
ICAM1	DHX37	MAML3	PLK1	ZNF688	LRRC45
GPRC5B	ANKRD44	MT-CYB	CHCHD3	TBC1D13	MCM5
CCL28	NDUFA13	UBALD2	POLR1B	TARBP2	SLC8A1
IGFBP7	RASSF5	MTRNR2L1	FASTKD2	WDR54	DOT1L
GNE	MT-ND4	EIF4E3	FANCD2	UBXN11	ZFAND2B
C3	AC138969.1	ALDH1A1	MVB12B	PCDH1	ALDH16A1
GBP2	MT-ATP8	MT-ND2	NME1-NME2	MAP4K2	ANKMY1
TNFAIP2	AGAP4	TP53INP2	C14ORF80	RHBDD3	TRMT112
PLA2G16	MT-ND5	GPC4	POLA2	NSL1	NDUFB6
C1S	NPHP3	MT-ND3	PHB2	PTPRE	ARHGEF10
SORBS2	DTNB	SORT1	WDR62	DSCAM	RPA1
MX1	AK9	FSTL1	THOC3	TRAF3IP3	DUSP7
AQP3	PEX5L	LMO7	UBE2C	PSD4	AP5Z1
RARRES3	PTN	TP53I11	NME1	NTPCR	FH
IGFBP4	KANK2	GATA3	MT1E	DDX39B	GINS4
GNL1	NDC1	GDPD3	PPIL1	MFSD13A	RPS6KA4
EPSTI1	AGAP2	NLRP10	PPIF	TRIM47	SNU13
IFIT1	PLAC8	PLA2G16	CASC4	XAB2	ACBD6
NLRP10	SCD	IFITM1	ZADH2	NAGS	DARS2
MT-ND1	INSIG1	IFI6	MARS2	HSPBAP1	PER2
TMOD1	MT-CYB	KLF9	RPS3A	CSNK2A3	GMNN
TP53INP2	PRRG3	ORAI2	MPDU1	ZNF235	FANCA
SMARCA1	IRX3	DNAH1	AURKB	ALOXE3	YRDC
MT-ND5	TCOF1	TIMP2	CDKN2C	SMYD3	TMPO
PTAFR	HAT1	LYPD3	MPP3	CYB561A3	IPO9
LMO7	SPATA17	KPNA7	DHRS4L2	SIK1	PA2G4
GCNT3	MT-ND2	MMP7	DLEU1	ABHD11	LAMTOR4
XAF1	ZNF571	PLSCR4	AFG1L	RAB6B	SLC2A4RG
MT-ND6	UTRN	MAF	PEF1	RFX7	HRAS
CCL5	EVI2B	ANGPT1	HERPUD1	SEC24D	C8ORF33
B3GNT7	MT-ND6	GBP2	PPIH	PHYH	KAT2A
SALL4	ARL6IP6	IL17RD	C12ORF73	ATP5J2-PTCD1	EIF3B
CADM4	CCDC191	PCDH12	MCM2	MAP3K6	RTN4IP1
TXNIP	NAV1	RARRES3	BIRC5	DUS1L	RAD18
GRHL1	KCNJ6	ABCG1	OSBPL6	ZNF514	KLHDC4
FKBP10	NEB	FMN1	CCNF	TRIM3	NCAPD2
KRTAP2-3	MT-CO3	DNAJC6	KIF23	LZTR1	DKC1
EVC2	YJEFN3	FGF23	FHOD3	PLEKHG4	TOMM22
ABCC2	PSIP1	ICAM1	MDP1	CEP170B	ECH1
DHX37	EDIL3	TMOD1	PUS1	TPRA1	PIGU
RHOF	WASHC2C	H1F0	DDT	SPHK1	CARS2
MT-ND4	GNAO1	HAP1	TUBA1C	AMTN	FUT10
LIPH	MT-ND1	MTRNR2L8	FAM173B	SQSTM1	FEZ1
PTPRR	TRAPPC2	CLDN1	DHODH	CERS2	ARMC5
ISG20	TRIM27	HEPHL1	TBCD	PI4KA	CAV1
DNMT3B	MT-CO2	RAET1E	KPTN	HAUS7	C14ORF159
ABCG1	TMEM123	PODXL	NHEJ1	HS3ST1	PDCD2L
INHBB	JDP2	PCSK5	NKX2-5	PLCD3	RNASEH2B
EFNA1	MDC1	CEACAM1	ACADVL	FASTK	DHX30
CORO1A	HEG1	EPSTI1	ADORA2B	NAT9	RAE1
LYPD3	RHBDL2	TTC9	TMEM11	MAMLD1	RPL11
CDK11B	MSMO1	TMOD2	RPS13	SKIV2L	AC015813.2
PHLPP1	C14ORF1	NPTXR	RPS4X	SERPINB2	LSM5
YJEFN3	EGLN3	YY2	EPN3	BACE2	UQCR10
IFI44L	CNTRL	LBH	PEMT	CNPY2	PPIH
ETNK2	SRRM5	EEF1A2	PMVK	MIB2	SULT1A1
CTSS	ESR1	TAGLN	RRP9	MYO18A	CWF19L1
KRT86	MNX1	PTAFR	RPA3	PWWP2B	RAB34
CXCL3	GALK1	CDK11B	RPLP0	FAXC	RRM2
FNBP1	HECTD1	LYPD5	SRM	SPOCK1	FANCD2
FGD3	CALB2	TNFSF10	RPP21	C16ORF91	POLR1A
SOX4	HMGCS1	PGM2L1	CHCHD5	MANBAL	TRAPPC12
TIMP2	SCEL	TFPI	RAN	FMNL2	MTERF3
PIGR	CLK1	TSPYL2	PRMT3	ADARB1	MRPL23
MINDY1	CYP51A1	AKAP8L	C19ORF48	UAP1L1	AKR7A2
CPED1	MED12L	CTSV	ZNF623	IMP4	DIP2A
FSBP	MMGT1	XAF1	MRPL13	CLCN5	CKS2
APOL1	CCDC14	CD74	MTERF3	FBXL15	DEF8

HEG1	CFI	CAMK2B	XAB2	MED17	MED16
MT-ATP6	ARPC4-TTLL3	GCNT3	TOMM40	SRSF8	MRPL20
MT-CYB	DMRT2	LGALS9	RPS7	OTUB2	NDUFAF1
TRIM27	MT-ND4L	IGFBP7	DNAAF5	TMEM8A	JAG2
COX6B2	MT-ND3	NAA30	SLC2A4RG	ADGRE2	GEMIN6
PFKFB4	LEAP2	LTBP2	DDB2	AC004832.3	SMPD4
HSD11B1	DZIP1L	MUC20	ATAD3B	DNER	KIF18A
SERPINA1	NEMF	TIAM2	COQ6	PORCN	WDR34
ANGPT1	BOC	TLR1	HADH	RCOR1	DNAAF5
TLR1	CFH	CCDC71L	LYRM7	ARMCX5	MACROD1
LTBP2	TSPYL2	YJEFN3	FAM207A	MRAS	XXYLT1
OAS1	ZNF821	ATP8B1	PRPF40A	SH3TC2	ESPL1
SCNN1A	ADD3	TUBA1A	BCKDHA	AC133555.5	BRCA1
AURKC	SH3YL1	ENO2	ATAD3A	ARHGEF40	ZNF202
SPP1	CBWD3	SATB1	POLD2	MIEF2	RABEPK
BATF2	C9ORF84	TPM1	RPSA	FEZ1	CRYBG3
CYB5R2	OTOGL	PBXIP1	PPAN	GPNMB	PRKAG1
ERV3-1	TMEM154	ANKRD24	POLR3H	ACADVL	LYRM4
DNAJB5	CDK11B	VPS13D	RPL6	KLHL21	CNOT6L
PCSK5	BLNK	BSPRY	ACAT1	S100A6	RACK1
APOLD1	KRI1	B4GALT6	MRPL53	RSRP1	MRPS24
MMP7	LRRCC1	MT-CO3	SLC25A14	ANKRD16	COG4
RDH10	MT-CO1	ERV3-1	DDX39A	FICD	MAD2L1
BSPRY	SLC25A27	MT-CO1	DYNC2H1	ZBTB17	NIP7
GPR160	ATP6V1G2-DDX39B	CMYA5	TRMT61A	ATG2A	DDX54
DUSP1	SCN3A	TXNDC15	DHRS4	HERPUD1	LSM6
CXCL11	FAM46A	SUGCT	HGH1	TBC1D30	COMMD4
LIPG	NRDC	ZNF708	NXT1	RAB11FIP4	ODC1
PLOD2	CCDC80	SLC16A13	ODC1	ST3GAL4	MRPS15
SORT1	FBN1	MT-CO2	SLFN11	AP5Z1	TMEM237
IFIT3	LAMC1	ZNF836	MRPL37	HYI	NME6
PLEKHA6	MPDZ	SHISA2	MRPL11	KCNMA1	DENND1B
PPM1M	FNBP1	CALB2	POLR2L	RBM15B	RPL27A
MTRNR2L8	ZCCHC8	SNED1	EEF2KMT	PLCE1	CENPM
HNF4G	MTRNR2L1	APOLD1	ADAMTS1	ANKRD28	NXT1
NECTIN4	CCDC77	ZNF506	ESPL1	IFI27L2	QSOX2
APOBEC3D	ATP8B3	LIMD2	UPP1	RAP1A	UQCRFS1
MITF	SLC6A9	NMNAT2	ATP5F1	BRD2	MINDY4
MGAT4A	NELFE	CDA	TYMS	SELENOT	POLR3B
NMNAT2	FADS1	PLOD2	TXNDC17	KIFC1	GSS
PRDM1	B4GALT6	PDGFB	RPL4	C8ORF33	ECE2
PLA2R1	FRYL	MFAP2	CTU2	EP400	GCSH
IL23A	USF3	BPGM	MRPL27	PTDSS1	ENTPD7
GAB2	RFTN2	RAB3B	CENPI	DUSP7	TRIP13
FMN1	KIAA0368	COL4A4	AC133555.5		NUDT8
SAMD9L	COL4A2	CELF6	MRTO4		CDCA5
MUC16	MEIS2	L1CAM	RFX7		AMER1
NEURL1	RASA2	LRRN1	TMEM241		DNAJA3
NFKBIZ	PIK3R1	CNGB3	BDKRB1		NCAPD3
MFAP2	COL12A1	OLFM2	TIMM10		CDT1
RND1	SEPT7	NMB	FAM185A		SSRP1
TTC9	TESMIN	TXNIP	SYBU		ZNF544
JPH2	TRAF3IP1	B3GNT7	THNSL1		TBC1D30
HERC5	KBTBD8	ATF3	RANBP1		MOCOS
NUPR1	BRSK1	PLEKHG2	DPH1		MRPS26
C15ORF48	PLEKHA4	TGOLN2	POLA1		ATP5F1
IFIT2	POLR3GL	TJP3	RTN4RL1		MARCH8
MT-ND3	TXNIP	SOX4	DDX49		ZNF138
CACNA1A	NFE2L3	SORBS2	ATP5G3		EEF2K
TDRD7	NUCB2	BVES	ZNF35		GNPDA1
PDGFB	TBC1D32	UPK2	AKAP8		CCDC150
TMEM25	MYO9B	EPPK1	CCNB1		SRA1
NTN4	LPAR6	GAB2	SIVA1		DPCD
S1PR1	GAS8	KIAA1551	AARSD1		GADD45GIP1
POU2F2	LENG8	KRT13	WDR4		MCM7
WFDC2	FAM184B	HIST1H2BD	PXMP2		PRDX2
CLIC3	FAM49A	NCCRP1	PTRH1		CPNE1
PLAC8	IQCK	MYO5C	GSTP1		RPS3
KPNA7		SREK1	AL591806.3		EPHX2
QPRT		ZNF518B	NUDT8		TONSL
GALNT6		GOLGA6L4	RPS12		MRPS27
ZNF750		TRAF1	VEPH1		GTF2I
EDN1		C3	ICOSLG		HSCB
TIMP3		MX1	PFKM		DHRS4
VASN		IL36RN	EMG1		BDKRB2
CALB2		ANOS1	BCL2		PMS2
SLC43A2		SEMA3F	HMGN2		BDKRB1
IL36RN		GABARAPL1	ING5		RPS14
TRPV4		C15ORF48	IMPDH2		NR2C2AP
VANGL2		GPM6A	NDUFA4		SRM
NMB		LIPH	MMS22L		GTF2H3
CLDN4		CCDC68	NRG1		PES1
ZEB2		GNAO1	MIPEP		ARL4D
USP18		PRRT2	RUVBL1		ALKBH3
SUN3		MARCH4	RAD51D		SLC43A3
TFPI		OLR1	TUBB		WRAP53
ABCD1		KLHL24	TLL1		DKK3
ST8SIA1		PARM1	METTL16		ZNF77

CMPK2		HSPE1-MOB4	TNPO3		RPL3
MPDZ		DUOXA1	H2AFZ		RPL7A
PAPSS2		TBX6	CARS2		LIG1
IGF2BP3		KCNN4	WDHD1		L3MBTL2
ARL11		AGO4	ATRIP		FPGT
MT-CO1		YPEL1	IL6R		CDC25A
DDX60		HOXC9	COMMD3		BOP1
TTLL3		RETREG1	POP5		POLR3E
FUT3		NIPSNAP2	ADSL		EIF3K
MT-ATP8		RNF32	RPAP1		COMMD9
MEX3A		SPP1	IAH1		WDR35
CFAP57		RUNX3	TDP1		RPL13
IL17RD		C10ORF10	TMEM161A		POLR2L
RIMS2		FBLN1	CDC25A		RPS29
PGM2L1		CTRC	POC1A		PTPRZ1
FGF11		ALDOC	EIF4A1		SLC25A20
CDA		VANGL2	POLE4		MRPS25
NXNL2		PGF	UROD		PHPT1
MT-ND2		ENPP1	ARMC6		BLM
FMNL1		VAMP2	CKMT1B		METTL16
LGALS9		BEX2	TMEM116		ATP23
YPEL3		MXRA5	TMEM14B		VPS51
INHBA		CD68	PI4KA		FAM173B
NDRG2		GPRC5B	ENOSF1		HINT2
TTN		PLA2G4C	MRPL40		MRPS34
CDH1		TMEM123	GEMIN6		MRPL43
LCN2		NECTIN4	RPTOR		DNA2
ZNF525		PTPRA	RBM14-RBM4		CHCHD6
MT-CO2		CCL5	ALOX12		ARHGAP11A
SLITRK6		DUSP1	GINS1		RPS10
SOD2		ECM1	CDH13		EME1
TSPAN13		LAT	PLA2G4A		H2AFX
SLC9A9		PARD6B	TMEM218		SKA3
VNN1		SERPING1	RNASEH2A		PPAN
TYMP		IL32	PBK		AVPI1
TNFSF13		BBS2	YBEY		PBK
PTPRA		MYO9B	PCNA		RRM1
HLA-B		STEAP4	GPR39		ATP5J
EPPK1		ITGB8	TIMM13		TRIP6
CNGB1		YPEL3	UMPS		MAN2C1
COL4A4		NUPR1	UQCC2		OIP5
IFITM2		ARGLU1	METTL8		SLC25A19
KLF9		HIST1H2BC	MRPS28		ATRAID
LOXL2		JUND	LEF1		DDX28
KRT13		MAP3K8	S100A2		RFC2
PEAR1		CAPS	STK11IP		PKP3
LRG1		ITM2C	CENPP		NDUFA9
TSPAN15		SEPT3	TRIM28		METTL8
AGO4		KIAA1462	PPA2		BCL2L13
PTPRJ		NFATC2	TUBA1B		TNPO3
IDO1		PRRG3	DCXR		H2AFV
CD38		STX11	TBC1D30		BABAM1
DDX58		CHD6	UNKL		ELOF1
ITGB8		REEP3	ARL4C		CKMT1B
LGMN		MAOA	SLC39A3		ATRIP
GSN		GPR132	ARHGEF1		ATP5O
ZNF780B		ATP12A	KIF26B		ZSCAN21
MOK		INHBA	CLUH		MAPK12
HEPHL1		ILDR1	GINS4		NME2
TVP23C-CDRT4		PAPSS2	RAB38		MYBL2
NOTCH3		FLNC	FLRT2		POC1A
ISG15		CCDC82	SLC37A2		POLD2
MTSS1		APH1B	CDK7		MLH3
LYPD5		RDH10	SNX5		C2ORF74
KIF13B		CCDC92	RRS1		RRP7A
MYO5C		MACF1	CENPO		KRT14
ARHGEF37		LIMCH1	TRAP1		MRPL13
MAP3K8		LGMN	SEPHS1		TMEM138
CYGB		AGPAT4	KITLG		PEX7
TRAF1		DYRK1B	IPO4		IFRD2
ZNF821		IFI44L	CCDC86		RRP1B
PRSS8		OAS1	NPR3		MUM1
ALDH3A1		PRSS8	UTP20		THOC1
TRANK1		SAMD9L	CDC20		NHEJ1
CDH5		LIPG	RING1		MECR
MYRF		MYH14	ZNF584		TELO2
SOCS3		IVL	PHF19		CDC25C
AC138811.2		STBD1	SLC25A5		GAPDH
ATF3		FAXDC2	BCS1L		KLHL22
TRIM38		ALDH3B2	PCDH7		LRR1
SAT1		PLEKHA6	UBE2G2		ATP5B
ITGA5		LY75	EIF3L		TMEM120B
OAS3		ZNF738	MRPS27		AGFG2
IGSF10		CACNA1A	HGSNAT		BUB1B
SHOX2		MAB21L3	PAAF1		MANEAL
LIMCH1		TMEM145	MRPL12		RPL22L1
NNAT		DLG4	ORC6		MMS19
FAXDC2		ARPC4-TTLL3	NCR3LG1		ZNF689
MT-CO3		FMNL1	EEF1AKMT1		WDR12

ZNF699		IGFL1	TTC26		FGFR2
SEMA3F		HIST2H2BE	PABPC4		EIF2B3
PPIC		ABAT	COPRS		NARS2
PXDN		NDRG2	SLC16A7		PEF1
A4GALT		NFKBIZ	XRCC3		URI1
ZNF738		KRT86	EARS2		NCAPH2
MMP10		PXDN	MFSD2A		ZNF25
MTRNR2L11		FCHSD1	ZRANB3		MCM10
CD74		SIX2	THADA		STARD3NL
A2ML1		FAM26E	DTYMK		ULK4
HAP1		IFIT1	DUS1L		KIF18B
WIPF1		DUSP5	CDK4		EXOSC8
DNAH2		A2ML1	TOE1		TMEM218
RUNX3		SHOX2	GINS2		MIPEP
TJP3		ZSCAN2	PLCE1		EXOC8
GDA		GATS	CCDC66		POLQ
ANKRD65		CORO1A	KIF4A		CCT7
AL136295.5		PRDM1	KRT5		NME1-NME2
YPEL2		TNFSF9	RBM15B		PMPCA
ENO2		MTRNR2L4	KCNJ15		PAAF1
CRABP2		HTR1D	ZNF26		HAUS4
CTSB		BHLHE41	ZBTB44		NDUFB2
ACVR2B		IL6	GSR		ATAD3A
SCARF1		A4GALT	C12ORF66		ZNF343
ZNF506		IGIP	IMPDH1		RNF123
EEF1A2		SUPT5H	CHTF18		DCUN1D2
SERPING1		SLC22A1	NCKAP5		EEF1AKMT1
GPC4		GCNT4	FAT4		ABLIM1
LRRN4		DBNDD1	NDUFAF8		SSSCA1
RAB11FIP1		CTGF	DUS3L		SRSF2
CHD6		ARID4A	WDR73		PPIA
IRAK2		N4BP3	SELENOT		RPUSD4
C10ORF10		PLD1	ERCC8		TUBB
NR4A1		LXN			REXO5
STBD1		SOX30			CIT
ZNF350		FBXO2			PTTG1
FOLR1		TTC39A			FIZ1
KBTBD8		CDH1			PABPC4
TP53I11		ZNF766			RTEL1
GPX7		HERC5			RIN1
NAA30		JDP2			CENPA
ACKR2		FLT4			PNPO
CFLAR		BNIPL			ARL4C
LBH		RSPH3			MRPL16
SGSM2		CLDN4			EMC9
CTH		KLK10			ZNF696
KANK2		ZFAT			DHRS4L2
ZNF518B		TM7SF2			DHX35
HOXA9		TNFSF13			HTD2
GMPR		RNF128			TTC19
CLSTN3		OSBP2			COPRS
PSCA		BATF2			SORD
TMEFF1		NNAT			PGAP2
PPFIA4		NEDD9			TMEM216
GIPR		ZNF681			FUS
BHLHE41		EVC2			MICB
RAB8B		CXCL14			NABP2
IL6		STIM1			ATP5SL
LLGL2		BMP4			POMK
POU2F3		ATP9B			BCL11B
ZNF365		ITSN2			SIVA1
IQCD		CYGB			CHCHD10
NEDD9		LRRC37A3			COX7B
ANGPT2		LMBR1L			CEP128
HOXC8		FGD3			PFAS
C16ORF54		INCA1			IDH3B
IGFN1		LRTOMT			UBE2T
CAVIN2		HHIPL1			METAP1D
TXNDC15		RPL39L			NOC2L
FAM26E		DNM1			AK2
LY75		CRYBG2			ITGB3BP
SIX2		SEMA5A			C16ORF59
TGM1		SULT1B1			RPS5
TRIB2		HSD11B1			L2HGDH
KLK10		MYO6			XAB2
NEBL		TNFAIP2			DTL
KCNN4		HMSD			RPL37A
KIAA1211L		MARCKSL1			SLC39A3
GDPD3		PIK3R3			CYP1A1
IL1R1		CNTN5			NDUFS2
DCAF4L1		CCDC73			TUBA1C
TIAM2		ERO1B			FAM98B
IFIH1		SMPD3			MPP3
ABCB5		KIAA1257			SUV39H1
RNFT2		EFNA1			STOML2
PARP14		MOSPD2			TACC3
NFKBIA		RORB			HS3ST3A1
OAS2		ID4			LRP8
GALC		SERPINF1			UCK2

CDKN2D		TSPAN2			RPS23
PCDHGA4		EDN1			TDP1
OXTR		RHOF			DPH1
TSPAN2		VMP1			ZNF655
DUSP5		STAT5A			CCDC86
UNC13D		MEIS3			PHF5A
ATL1		CCL28			HADH
CASC10		TDRKH			C11ORF1
RHOV		ITIH6			MED24
SLC2A12		PPP1R3B			MKS1
AGPAT4		TNFRSF10C			RPS16
FAM193B		IL2RG			NDUFAB1
APCDD1L		LGALSL			FAM173A
ERVW-1		PNRC1			ATP5G3
SYTL2		QPRT			EXD2
RNF157		TRPC1			RNF31
ZNF583		GOLM1			C6ORF141
DMPK		YPEL2			DSN1
MME		FARP1			MRPS28
AL365205.1		HHEX			TYMS
TMEM27		MME			ORC1
UBALD2		ADRA1B			NDUFS7
FGF13		ZNF468			COPS9
MT-ND4L		SERPINB7			RFC4
HYAL1		LRG1			FAM216A
DNAJC22		SIAE			RPL34
ARL14EPL		MLF1			TK1
THEMIS2		ARL14			PMF1
NFE2L3		KBTBD8			STUB1
TMEM98		TGFBR3			TRA2B
BCL2A1		RAB3IP			FAM196B
KIAA1257		TMEFF1			CCT4
BNIPL		VAV1			FEN1
PLAG1		GJB4			FAH
NPHP3		BTBD19			ZNF74
HELZ2		FNBP1L			SCLY
TMEM123		FGF11			TMEM192
CD68		FAM25A			FASTKD2
ADGRF1		PHYHIP			E2F1
IGFBP3		VGLL3			PRMT3
TNFSF9		LSM14A			MRPS17
PGPEP1		FSIP2			SMYD3
PNPLA3		IL23A			FBXO4
SLC25A37		WIPI1			NUDCD2
SLC16A4		FUT2			SLC25A15
PNRC1		SDR16C5			RPTOR
CD274		RGPD6			PSMA1
STAT1		ABCD1			DNAJC11
PKIB		TRPV4			ZNF511
ABAT		ARHGAP31			NCR3LG1
ALDOC		MMP10			ABCB6
ARHGAP27		SLC16A4			EEF1A1
HSPE1-MOB4		HOXB6			EXO1
CLDN7		TRIM38			ATP5G1
SYNGR3		SCEL			THOC3
DTNB		DNAJC22			C14ORF80
FGF14		ZNF677			SNRNP40
PLA2G4C		WDR45			FAAP24
RCAN1		VGLL1			TIMM44
GLRX		PIWIL2			NOC4L
COBL		HEG1			TBRG4
NDRG4		IL11			IPO11
CENPT		IGFBP4			HMGN2
CES3		SLCO1A2			NUBPL
RAET1L		ECE1			HSPD1
SLC12A7		TNFRSF6B			HIRIP3
GABRP		ZNF365			KIF26B
HTR1D		STAG3			RBM34
MAOA		PAPPA			RTN4RL1
ATF5		NPBWR1			LSM7
IFNLR1		TRIM2			CENPP
OSBP2		STX2			RPS27A
ATP12A		RAG1			DLST
IL24		PIK3IP1			TRAPPC9
SERPINF1		ATF7IP2			SLC16A14
VGLL3		PTTG1IP			LGALS1
LMBR1L		AC138969.1			RAD9A
C10ORF55		DDX60			IMPDH1
HOXB3		EFCAB13			TIMM8A
CXCL2		ATP2B4			SRSF7
LTBP1		MGAT4A			PIF1
LGI4		TMC8			PINX1
MYL9		AQP3			FOXM1
MAB21L3		C2CD2L			TOMM6
YY2		IRX5			NME1
FGF5		WFDC2			C7ORF50
BMP6		NTN4			AGPAT1
GOLM1		BMPR2			SETD6
PARP9		CYB5R2			TOMM40

GABARAPL1		TSPAN13			RPS2
ZC3H12A		KIAA1211L			DLEU1
CREG2		PSCA			NPRL2
DUOXA1		PDZK1			MAIP1
TMPRSS4		HOXB3			RPLP0
BPGM		SP140			TXNRD2
ALPP		PHLPP1			ZNF165
CASZ1		NEGR1			C12ORF45
AC138969.1		NREP			LPAR3
OASL		LZTS3			PHF19
PCED1B		SLC8B1			NOB1
PLSCR1		DNAJB2			PEMT
OSMR		ALPP			TMEM201
TRPC1		LRIF1			ALOX12
SWT1		MEX3A			USP47
GPR132		S1PR1			UTP20
MTRNR2L4		NEK11			CCNB2
PDZK1		PROS1			DUS3L
TNFRSF10C		ACKR2			DLX1
KRT6B		GRHL1			RPA3
FAM46B		LRRC4			TRIM7
SLC12A6		RABL2A			ACAT1
L1CAM		ZEB1			LIX1L
ELF3		SOD2			AGMAT
SPRR2E		MSC			RPL14
GATS		IFITM2			PTDSS1
TAGLN		AMZ1			CDCA2
HOXB6		POLR3GL			KRT10
PIPOX		GNE			ERVMER34-1
ACTBL2		CDC14A			USF1
AFF1		Z98749.3			RPL10A
PIK3IP1		MMAA			ARMCX5
GPR158		MYRF			GSDMD
BTBD19		HOXB8			GEMIN5
RABL2A		MYPN			PRPF19
TAB2		CCPG1			PTHLH
PIWIL2		STX3			TAF5
SYCP2L		APCDD1L			CYC1
ACE2		MAPK15			PAICS
PAPPA		RCAN1			CKMT1A
ERBB3		LCN2			SNRPD1
FBXW10		DBNDD2			NDUFAF6
SERPINB1		CPT1A			ADORA2B
IRF9		CTF1			KIF2C
ZNF223		LMBRD1			TTLL11
PARP12		PCED1B			POLR1C
PADI1		FILIP1L			NPM3
ALPPL2		TRIML2			MRPL3
RALGAPA2		HOXA9			GPSM2
HAPLN3		SSPN			EARS2
IL4I1		WISP3			RAD51
SLC28A3		ARL11			ACADVL
CRISPLD2		CT62			MRPL55
APOD		LEPR			RPL35A
CHD2		LIN7B			PRR5
RAB15		CASZ1			UBE2G2
LRRC4		SYTL2			NDUFC1
RBM38		GIPR			PEPD
IL32		ERBB3			CAD
COL28A1		GDNF			THNSL1
ADAP2		GCC2			ORC6
CERS4		KIF13B			MCM4
LRRC37A3		HYAL1			PPA2
IL36G		VLDLR			GSTO2
PLEKHA4		ITM2B			POLD1
WNT4		SNAP23			GCDH
DNAJC6		SLC12A7			SFXN2
PARD6B		CCDC62			MECOM
ECM1		ADA2			RPAP1
TMEM97		ADCY9			RPS3A
SPINK9		GGT1			RAB38
ARPC4-TTLL3		LEPROT			RPL6
PPP1R3B		CHST2			PIGL
CTC1		KLK7			HMBS
ZNF626		RNF19A			MT1E
CLK4		TNFRSF9			PCNA
SDR16C5		GALNT6			ADAMTS1
NPIPA5		USP53			WDR54
HOXD13		CDK11A			XRCC3
STX2		PPIC			TIMM13
FBXO39		ABCA13			SF3A3
SCARB1		ATG16L2			IMP4
IL1RL1		SLC2A12			BCS1L
PREX1		ITGA5			PRKAR1B
SKIL		CXORF36			PRMT1
DENND3		RBM5			SNF8
NEK5		PPM1H			EPN3
FBXO2		RAB11FIP1			POLE4
HIST1H2AC		AKAP13			CCDC51

ITSN2		HAT1			ERMAP
RILP		CLU			ECSIT
TCP11L2		CFAP53			EBNA1BP2
APOBR		ZNF432			IMP3
TMC8		TMEM52B			PHKA1
RTKN2		C1S			TUBE1
CEACAM1		PPP1R2			BLOC1S1
ASPHD1		CFLAR			NOP56
OPN3		MYL9			KIF22
LGALSL		RAB7A			CCT8
RPL39L		RAET1L			CCNA2
HIST1H2BC		PPFIA4			EIF2B5
ACPP		INHBB			DLL1
SLC16A13		KANK2			GLYR1
PGF		ABHD8			ITFG2
FNBP1L		COL5A1			DNPEP
VAV1		ATF5			C19ORF48
CCDC71L		COX6B2			AHSA1
ADAMTSL4		HLA-B			RNASEH2A
SAMHD1		FAM214B			S100A2
PTGS2		SPINK9			COQ3
ABHD8		FOXL2NB			RAD54L
DUOX2		ABCC2			EIF5A
ZFAT		KCNJ3			MRPS2
ECE1		KDM6B			UBE2C
KRT16		ZDHHC11			ERI3
TAGAP		GALC			GRK5
SMIM22		LENG8			MRPL37
ADCY9		LTBP1			WDHD1
IRF7		YPEL5			CDCA3
SAV1		IGFN1			POLR1E
GLIPR1L2		NEBL			H2AFZ
S100A4		STC1			UPP1
JUND		ATP13A2			RPS21
ARGLU1		CYTH1			PSMG3
HECTD1		CREBRF			TRIM34
PSG9		SLC4A5			C1ORF109
RFTN2		TFAP2E			RPLP2
CCDC144A		XKRX			TRMT1
UNC79		VASN			CIDEB
IL22RA1		CMPK2			FBL
RASA4		FAM49A			MT2A
CA13		CERCAM			RANBP1
TRIM2		ACAD11			NDUFAF5
VPS13D		CHIC2			WDR74
DOCK8		FGF14			FAAP20
SCHIP1		MFGE8			CDC45
PSTPIP2		GFPT2			CRADD
NCCRP1		ALDH3A1			LARS2
GALM		TAB3			NCAPH
MYPN		PPP1R3F			MRPL11
IFI44		DCAF4L1			TUBA1B
HBE1		IGF2BP3			PHKG2
SIRPB2		TNFSF15			SMYD5
CREB5		ADD3			NPR3
CTCFL		TDRD7			MTHFD1
NAA60		IFIH1			EIF4A1
IGFL1		F2R			WDR4
NLGN2		HIVEP1			C1QBP
CLDN16		ARL14EPL			POLR1B
SREK1		SCNN1A			CTPS1
TNS2		C9ORF72			MCM2
AMZ1		DTX3L			MTFP1
MAFF		UPK3B			DCTPP1
EFCAB10		MARCH3			CCNB1
GADL1		CSAG3			BIRC5
FSIP2		CDH5			TRAP1
ARRB2		BEND7			SKIV2L
MYADM		PTP4A3			ATAD3B
CDR2L		PADI1			RRS1
KLF15		ZFYVE1			RPL37
RABGAP1L		ZHX1-C8ORF76			PLK1
CPA4		DOK3			PCDH7
COL8A2		RHOV			RPL22
KIAA1551		COL4A2			KIAA0586
ZNF615		MLPH			PCLAF
PDE8A		ZNF615			NCLN
HIST1H2BD		USP2			GPAM
FUT6		MYADM			RPS7
ZNF714		NPTX1			NRG1
SDC4		APOBEC3D			RPS12
TMEM217		PDE1C			BUB1
BEX2		SWT1			PHB2
DPP3		UBL3			AURKB
GLIS3		PLAUR			CLUH
SHISA4		RAET1G			ZC3HC1
CREBRF		ATL1			NDUFS3
ZNF217		DHX37			MRPL22
LPCAT4		FAM102B			FJX1

HOXA5		IST1			DTYMK
ABCA1		HOXB2			PDSS1
EPHX3		MMP13			FARS2
UPK2		TYMP			TLL1
SH3D21		POM121			SLC37A2
ZSCAN2		PDZD7			PRMT7
ATF7IP2		SAT1			CNOT10
CDK11A		PTGS2			NDUFAF8
LEPR		XKR4			CENPO
CHMP5		FNDC3B			NOLC1
EPCAM		VSIG10			CENPX
DTX3L		EPN2			TRMT61B
RNF19A		PPM1N			BACE2
PLAUR		FOLR1			PSMB6
ZNF224		TMEM106B			GPHN
FRK		ABCA1			EMG1
SPATA20		PPM1J			DDX39A
SOWAHB		FOXN3			TADA1
ANKRD26		SLC16A3			SLC25A10
ZNF432		NEURL1B			EHBP1
RAG1		TEX35			CDCA7
FBP2		SERPINB1			SHCBP1
SP140		RASSF5			MCAT
SMPD3		HOXB4			UQCC2
VAMP2		N4BP2L1			SPC25
STEAP1B		CCDC186			PDF
TMCC3		PSTPIP2			HGH1
BRSK1		RHOQ			RPSA
TFAP2E		FLT1			KRBOX4
CCPG1		GPR89B			URB2
TNFAIP3		NXNL2			RRP9
TDRKH		HYAL4			PI4KA
RAB3B		MAFF			MCM6
ERO1A		EPB41			CC2D2A
ENKUR		SLCO4C1			GINS2
ZFP14		PPM1M			PLCE1
DLG4		DSC2			METTL17
MEIS3		LOXL3			CDK4
SAMD9		CD274			TRIM28
B4GALT1		GGT6			LYSMD2
CPEB3		SERPINB9			DHODH
DOK3		C7ORF57			MPHOSPH9
		MTRNR2L11			RPS4X
		RERE			MPDU1
		SLC12A2			KIF20A
		SYCP2			NUDT6
		DNAH5			SNX5
		SKIL			FAM58A
		HIST1H2AC			SLFN11
		HIST1H2BJ			TFAP4
		DOCK8			KITLG
		ZNF813			SLC16A7
		CPED1			MRPL40
		FAM214A			RBM15B
		KIF27			BLMH
		KATNAL1			MRTO4
		NPAP1			VOPP1
		ALOX5			KLHL13
		ZNF354A			FUNDC1
		PTPRJ			SLC25A5
		TMEM27			C20ORF27
		ZNF43			RFX7
		IFNLR1			MRM3
		C10ORF55			PUS1
		TRPA1			MRPL48
		SLC7A2			EEF2KMT
		LRRC56			KRT5
		VNN1			FANCB
		CALCOCO1			RPS13
		GRIK2			PLD6
		ZMYM5			GINS1
		SPECC1L-ADORA2A			NUP88
		RNF182			MRPL58
		ZSCAN30			CENPL
		ARRB2			NCEH1
		PKIA			PLA2G4A
		PARP9			METTL1
		TSPAN14			LMNB1
		L1TD1			MRPL12
		ZNF844			PFKM
		RBP7			GSR
		TMEM133			GTF2H2
		ZNF611			CDC20
		HEY1			GTPBP6
		DAPK1			MYBBP1A
		KLHL6			GAR1
		NDC1			MPV17
		FGF5			IMMP1L

		FUT4			POP4
		CPEB2			MRPS6
		OAS3			RFC5
		CLK1			PPM1G
		ZNF750			ANAPC5
		ZNF292			IPO4
		CAPN5			MYCBP2
		UBE2D1			AKR1C2
		ARHGEF37			COMMD3
		KDELR3			CENPW
		ISG20			EBPL
		ZFHX2			EIF3L
		SSC4D			TXNDC17
		PADI3			RPS17
		PLA2G7			RAN
		SLC44A2			SELENOT
		CLIC4			RPL4
		AC091167.3			
		TMEM38A			
		SERPINE2			
		NRDC			
		HOXC8			
		PLAG1			
		MDM2			
		HOXC6			
		TMPRSS4			
		STAT1			
		SLC28A3			
		PCDHGA11			
		MELTF			
		TSPAN6			
		CDKN2D			
		BTG1			
		ICA1			
		COL1A2			
		ENTPD2			
		CTTNBP2NL			
		GLRX			
		EPB41L5			
		TMEM97			
		MINDY1			
		FAM107B			
		ARHGEF28			
		ZEB2			
		ZNF563			
		FYN			
		SLCO2A1			
		CCDC17			
		HOXA13			
		PLAC8			
		BMP6			
		PARP14			
		KRT16			
		IFIT3			
		PLA2R1			
		HIC1			
		MAP1LC3B			
		CTSB			
		ULBP2			
		MT-ND4L			
		ANKIB1			
		DOPEY2			
		ARL8A			
		PRSS27			
		TTC28			
		AURKC			
		MCF2L2			
		KATNBL1			
		IL4I1			
		MLLT3			
		UBN1			
		UNC5B			
		GLDC			
		JPH2			
		ABCA7			
		TMEM45A			
		ASTN2			
		HAL			
		AC005324.3			
		APOD			
		PLPP6			
		PRODH			
		ZNF350			
		CLDN16			
		APOL1			
		KIF3C			
		EBLN2			
		TIMP1			
		USP18			

		ETV1			
		SMPDL3B			
		AZI2			
		ZNF185			
		VIM			
		BNIP3L			
		ZNF600			
		SH3BP2			
		IQCD			
		SLC43A2			
		KLRD1			
		OPN3			
		PDE8A			
		OSMR			
		PMEPA1			
		B3GALT5			
		TCP11L2			
		SLC44A3			
		SLC9A3R2			
		ANKRD65			
		PPARD			
		PLSCR1			
		SERPINI1			
		TMEM59			
		FAM46B			
		OCLN			
		NOTCH3			
		CAMK2N1			
		TBC1D8B			
		ZYG11A			
		ANO8			
		RP2			
		DAB2			
		TRIB2			
		GSTT2B			
		LGI4			
		SNX10			
		MOK			
		CPT1C			
		B3GNT3			
		SCARB1			
		MPZL3			
		IFITM10			
		CCDC39			
		CEP192			
		MICAL1			
		C1QTNF9			
		ADGRV1			
		MYO5B			
		CIR1			
		KCNJ2			
		APP			
		TMEM213			
		IL1RL1			
		NFKBIA			
		HBP1			
		CERS4			
		CREB5			
		ADAP2			
		TUSC3			
		CTSO			
		NPIPA2			
		REPS2			
		SV2B			
		AP3B2			
		SOHLH2			
		TMCC2			
		SPATA20			
		ZNF821			
		KRT9			
		S100A4			
		CLCN4			
		CDKL5			
		UBE2B			
		DTNA			
		DPYSL2			
		DHX57			
		GNL1			
		CASC10			
		SAV1			
		GLIS3			
		IL24			
		ZNF221			
		ZNF467			
		DYSF			
		TCF7L2			
		FLRT3			
		TMEM86A			
		MYRFL			

		COL5A3			
		ITGB7			
		VSIG10L			
		CPA4			
		ZFP28			
		TMEM159			
		KIAA1211			
		SYT11			
		NPIPA1			
		ZNF699			
		TP53INP1			
		RRM2B			
		ASPHD2			
		BEX5			
		RAP1GAP			
		LOXL2			
		CDKL2			
		FAM32A			
		MGLL			
		ZNF391			
		B4GALT1			
		EPCAM			
		KIAA1328			
		CTH			
		LLGL2			
		YIPF4			
		LRCH4			
		ACP7			
		ABCB5			
		MARK3			
		CHMP5			
		TRIM36			
		CLIC3			

Table S4. Full list of GO terms from REVIGO for differentially expressed groups.

Increased by Treatment								
DAC			Para			DAC+ Para		
term ID	description	log_{10} p-value	term ID	description	log_{10} p-value	term ID	description	log_{10} p-value
GO:0060337	type I interferon signaling pathway	-13.79	GO:0022904	respiratory electron transport chain	-11.15	GO:0019221	cytokine-mediated signaling pathway	-6.73
GO:0045071	negative regulation of viral genome replication	-9.20	GO:0032981	mitochondrial respiratory chain complex I assembly	-6.23	GO:0052548	regulation of endopeptidase activity	-6.40
GO:0048660	regulation of smooth muscle cell proliferation	-4.88	GO:0006754	ATP biosynthetic process	-2.71	GO:0048523	negative regulation of cellular process	-4.50
GO:0032069	regulation of nuclease activity	-4.43	GO:1902930	regulation of alcohol biosynthetic process	-2.64	GO:0030198	extracellular matrix organization	-3.82
GO:0031325	positive regulation of cellular metabolic process	-4.27	GO:0015988	energy coupled proton transmembrane transport, against electrochemical gradient	-2.53	GO:0045601	regulation of endothelial cell differentiation	-3.14
GO:0042775	mitochondrial ATP synthesis coupled electron transport	-3.93	GO:0044782	cilium organization	-2.46	GO:0045953	negative regulation of natural killer cell mediated cytotoxicity	-3.14
GO:0017157	regulation of exocytosis	-3.56	GO:0045787	positive regulation of cell cycle	-2.44	GO:0043691	reverse cholesterol transport	-2.99
GO:0001818	negative regulation of cytokine production	-3.53	GO:0046578	regulation of Ras protein signal transduction	-2.30	GO:1905037	autophagosome organization	-2.98
GO:0010642	negative regulation of platelet-derived growth factor receptor signaling pathway	-2.81	GO:0048864	stem cell development	-2.25	GO:0007009	plasma membrane organization	-2.90
GO:0001990	regulation of systemic arterial blood pressure by hormone	-2.71	GO:0006636	unsaturated fatty acid biosynthetic process	-2.20	GO:1902003	regulation of beta-amyloid formation	-2.87
GO:0055091	phospholipid homeostasis	-2.59	GO:0052547	regulation of peptidase activity	-2.05	GO:0048678	response to axon injury	-2.79
GO:0001911	negative regulation of leukocyte mediated cytotoxicity	-2.59	GO:1901570	fatty acid derivative biosynthetic process	-1.82	GO:0042775	mitochondrial ATP synthesis coupled electron transport	-2.74
GO:0045216	cell-cell junction organization	-2.57	GO:0001501	skeletal system development	-1.59	GO:0044257	cellular protein catabolic process	-2.66
GO:0030865	cortical cytoskeleton organization	-2.56	GO:0070534	protein K63-linked ubiquitination	-1.48	GO:0006501	C-terminal protein lipidation	-2.63
GO:0033273	response to vitamin	-2.45	GO:0046782	regulation of viral transcription	-1.42	GO:0003180	aortic valve morphogenesis	-2.54
GO:0030198	extracellular matrix organization	-2.39				GO:0048485	sympathetic nervous system development	-2.19
GO:0016338	calcium-independent cell-cell adhesion via plasma membrane cell-adhesion molecules	-2.35				GO:0055091	phospholipid homeostasis	-2.19
GO:0015988	energy coupled proton transmembrane transport, against electrochemical gradient	-2.32				GO:1990000	amyloid fibril formation	-2.19
GO:0097067	cellular response to thyroid hormone stimulus	-2.32				GO:0032530	regulation of microvillus organization	-2.19
GO:0016042	lipid catabolic process	-2.28				GO:0043116	negative regulation of vascular permeability	-2.19
GO:0006006	glucose metabolic process	-2.27				GO:0050918	positive chemotaxis	-2.10
GO:0009435	NAD biosynthetic process	-2.20				GO:0060037	pharyngeal system development	-2.10
GO:0007009	plasma membrane organization	-2.16				GO:0033273	response to vitamin	-2.05
GO:0010745	negative regulation of macrophage derived foam cell differentiation	-2.01				GO:0044267	cellular protein metabolic process	-2.03
GO:0046457	prostanoid biosynthetic process	-2.01				GO:0018146	keratan sulfate biosynthetic process	-1.96
GO:0071985	multivesicular body sorting pathway	-2.01				GO:0030865	cortical cytoskeleton organization	-1.96
GO:0071360	cellular response to exogenous dsRNA	-2.01				GO:0015718	monocarboxylic acid transport	-1.95
GO:0036152	phosphatidylethanolamine acyl-chain remodeling	-1.95				GO:0015988	energy coupled proton transmembrane transport, against electrochemical gradient	-1.92
GO:0048485	sympathetic nervous system development	-1.77				GO:0010941	regulation of cell death	-1.88
GO:0051258	protein polymerization	-1.77				GO:0016050	vesicle organization	-1.84
GO:0044267	cellular protein metabolic process	-1.73				GO:0048169	regulation of long-term neuronal synaptic plasticity	-1.81
GO:0034375	high-density lipoprotein particle remodeling	-1.70				GO:0033013	tetrapyrrole metabolic process	-1.78
GO:0050918	positive chemotaxis	-1.70				GO:0009235	cobalamin metabolic process	-1.78
GO:0015919	peroxisomal membrane transport	-1.69				GO:0006892	post-Golgi vesicle-mediated transport	-1.75

GO:0017196	N-terminal peptidyl-methionine acetylation	-1.69				GO:0045216	cell-cell junction organization	-1.74
GO:0043471	regulation of cellular carbohydrate catabolic process	-1.69				GO:0009435	NAD biosynthetic process	-1.72
GO:0032347	regulation of aldosterone biosynthetic process	-1.69				GO:0090329	regulation of DNA-dependent DNA replication	-1.71
GO:0031397	negative regulation of protein ubiquitination	-1.59				GO:1901264	carbohydrate derivative transport	-1.71
GO:0030388	fructose 1,6-bisphosphate metabolic process	-1.58				GO:0014821	phasic smooth muscle contraction	-1.71
GO:0015677	copper ion import	-1.58				GO:0046457	prostanoid biosynthetic process	-1.62
GO:0006357	regulation of transcription from RNA polymerase II promoter	-1.54				GO:0010224	response to UV-B	-1.62
GO:0071493	cellular response to UV-B	-1.48				GO:0006706	steroid catabolic process	-1.62
GO:0035563	positive regulation of chromatin binding	-1.48				GO:0044272	sulfur compound biosynthetic process	-1.59
GO:0006501	C-terminal protein lipidation	-1.41				GO:0006357	regulation of transcription from RNA polymerase II promoter	-1.52
GO:0048015	phosphatidylinositol-mediated signaling	-1.41				GO:0010107	potassium ion import	-1.50
GO:0046323	glucose import	-1.39				GO:0043471	regulation of cellular carbohydrate catabolic process	-1.42
GO:0051180	vitamin transport	-1.37				GO:0034375	high-density lipoprotein particle remodeling	-1.33
GO:0006654	phosphatidic acid biosynthetic process	-1.35				GO:0051289	protein homotetramerization	-1.31
GO:0035418	protein localization to synapse	-1.31				GO:0030050	vesicle transport along actin filament	-1.31
						GO:2000427	positive regulation of apoptotic cell clearance	-1.31

Decreased by Treatment

DAC			Para			DAC+ Para		
term ID	**description**	**log_{10} p-value**	**term ID**	**description**	**log_{10} p-value**	**term ID**	**description**	**log_{10} p-value**
GO:0034645	cellular macromolecule biosynthetic process	-11.94	GO:0046512	sphingosine biosynthetic process	-2.85	GO:0042254	ribosome biogenesis	-35.37
GO:0042254	ribosome biogenesis	-9.79	GO:0042759	long-chain fatty acid biosynthetic process	-2.76	GO:0016072	rRNA metabolic process	-31.32
GO:0006259	DNA metabolic process	-9.53	GO:0043604	amide biosynthetic process	-2.53	GO:0010467	gene expression	-25.56
GO:0000082	G1/S transition of mitotic cell cycle	-8.29	GO:0046474	glycerophospholipid biosynthetic process	-2.39	GO:0006259	DNA metabolic process	-23.50
GO:0016072	rRNA metabolic process	-8.13	GO:1901888	regulation of cell junction assembly	-2.34	GO:0019083	viral transcription	-22.59
GO:0006261	DNA-dependent DNA replication	-8.04	GO:0034976	response to endoplasmic reticulum stress	-2.32	GO:0000956	nuclear-transcribed mRNA catabolic process	-18.64
GO:0016032	viral process	-6.75	GO:0000187	activation of MAPK activity	-2.17	GO:0006281	DNA repair	-18.24
GO:0006614	SRP-dependent cotranslational protein targeting to membrane	-6.10	GO:0006940	regulation of smooth muscle contraction	-2.00	GO:0006414	translational elongation	-17.28
GO:0022616	DNA strand elongation	-5.93	GO:0044271	cellular nitrogen compound biosynthetic process	-2.00	GO:0000082	G1/S transition of mitotic cell cycle	-8.95
GO:0007005	mitochondrion organization	-5.91	GO:0051128	regulation of cellular component organization	-1.90	GO:0015949	nucleobase-containing small molecule interconversion	-6.96
GO:0002181	cytoplasmic translation	-5.89	GO:0048146	positive regulation of fibroblast proliferation	-1.84	GO:0009168	purine ribonucleoside monophosphate biosynthetic process	-6.96
GO:0010467	gene expression	-5.49	GO:0045070	positive regulation of viral genome replication	-1.76	GO:1901796	regulation of signal transduction by p53 class mediator	-6.87
GO:0000956	nuclear-transcribed mRNA catabolic process	-4.96	GO:0034660	ncRNA metabolic process	-1.68	GO:0090305	nucleic acid phosphodiester bond hydrolysis	-6.47
GO:0006415	translational termination	-4.90	GO:0000422	mitophagy	-1.55	GO:0006839	mitochondrial transport	-6.36
GO:0009168	purine ribonucleoside monophosphate biosynthetic process	-4.63	GO:0001764	neuron migration	-1.55	GO:0061641	CENP-A containing chromatin organization	-6.01
GO:0006414	translational elongation	-4.58	GO:1901566	organonitrogen compound biosynthetic process	-1.54	GO:0000732	strand displacement	-4.44
GO:0015949	nucleobase-containing small molecule interconversion	-4.02	GO:0050708	regulation of protein secretion	-1.50	GO:0006479	protein methylation	-4.41
GO:0006283	transcription-coupled nucleotide-excision repair	-3.98	GO:0006526	arginine biosynthetic process	-1.36	GO:1904666	regulation of ubiquitin protein ligase activity	-4.38
GO:0006839	mitochondrial transport	-3.74	GO:0001765	membrane raft assembly	-1.36	GO:0009411	response to UV	-4.26
GO:1904666	regulation of ubiquitin protein ligase activity	-3.71	GO:0031076	embryonic camera-type eye development	-1.36	GO:0006362	transcription elongation from RNA polymerase I promoter	-4.22
GO:0006336	DNA replication-independent nucleosome assembly	-3.55	GO:0016311	dephosphorylation	-1.34	GO:0051302	regulation of cell division	-3.93

GO:0044267	cellular protein metabolic process	-3.51	GO:0006470	protein dephosphorylation	-1.33	GO:0006360	transcription from RNA polymerase I promoter	-3.75
GO:0000731	DNA synthesis involved in DNA repair	-3.39	GO:0043484	regulation of RNA splicing	-1.31	GO:0034982	mitochondrial protein processing	-3.53
GO:0097033	mitochondrial respiratory chain complex III biogenesis	-3.33	GO:0035357	peroxisome proliferator activated receptor signaling pathway	-1.30	GO:0006353	DNA-templated transcription, termination	-3.32
GO:0009411	response to UV	-3.20	GO:0045714	regulation of low-density lipoprotein particle receptor biosynthetic process	-1.30	GO:0051188	cofactor biosynthetic process	-3.06
GO:0018022	peptidyl-lysine methylation	-2.74	GO:0042780	tRNA 3'-end processing	-1.30	GO:0040029	regulation of gene expression, epigenetic	-2.83
GO:0060249	anatomical structure homeostasis	-2.74	GO:0035280	miRNA loading onto RISC involved in gene silencing by miRNA	-1.30	GO:1904874	positive regulation of telomerase RNA localization to Cajal body	-2.67
GO:2001234	negative regulation of apoptotic signaling pathway	-2.55	GO:0010561	negative regulation of glycoprotein biosynthetic process	-1.30	GO:0001522	pseudouridine synthesis	-2.67
GO:0000959	mitochondrial RNA metabolic process	-2.47	GO:0010988	regulation of low-density lipoprotein particle clearance	-1.30	GO:0044806	G-quadruplex DNA unwinding	-2.64
GO:0042148	strand invasion	-2.25				GO:0006352	DNA-templated transcription, initiation	-2.49
GO:0043497	regulation of protein heterodimerization activity	-2.25				GO:0006396	RNA processing	-2.34
GO:0036297	interstrand cross-link repair	-2.24				GO:0006354	DNA-templated transcription, elongation	-2.22
GO:0019395	fatty acid oxidation	-2.18				GO:0000959	mitochondrial RNA metabolic process	-2.21
GO:0006362	transcription elongation from RNA polymerase I promoter	-2.07				GO:0048709	oligodendrocyte differentiation	-1.81
GO:0008213	protein alkylation	-2.03				GO:0032456	endocytic recycling	-1.76
GO:0045333	cellular respiration	-1.99				GO:0051181	cofactor transport	-1.74
GO:0006576	cellular biogenic amine metabolic process	-1.97				GO:0016236	macroautophagy	-1.72
GO:0072321	chaperone-mediated protein transport	-1.97				GO:0033688	regulation of osteoblast proliferation	-1.66
GO:0006360	transcription from RNA polymerase I promoter	-1.88				GO:0019218	regulation of steroid metabolic process	-1.66
GO:0032780	negative regulation of ATPase activity	-1.82				GO:0009749	response to glucose	-1.54
GO:0014032	neural crest cell development	-1.81				GO:0033119	negative regulation of RNA splicing	-1.53
GO:0051302	regulation of cell division	-1.80				GO:0015838	amino-acid betaine transport	-1.50
GO:0015985	energy coupled proton transport, down electrochemical gradient	-1.76				GO:0002903	negative regulation of B cell apoptotic process	-1.50
GO:0006084	acetyl-CoA metabolic process	-1.70				GO:0097384	cellular lipid biosynthetic process	-1.50
GO:0006352	DNA-templated transcription, initiation	-1.69				GO:0042148	strand invasion	-1.50
GO:0006353	DNA-templated transcription, termination	-1.68						
GO:0090305	nucleic acid phosphodiester bond hydrolysis	-1.63						
GO:0090181	regulation of cholesterol metabolic process	-1.63						
GO:0000377	RNA splicing, via transesterification reactions with bulged adenosine as nucleophile	-1.62						
GO:0006312	mitotic recombination	-1.51						
GO:0006266	DNA ligation	-1.51						
GO:0010501	RNA secondary structure unwinding	-1.50						
GO:0006301	postreplication repair	-1.48						
GO:0009081	branched-chain amino acid metabolic process	-1.35						
GO:0009451	RNA modification	-1.33						

Table S5. cBioPortal RNA-seq data (for cancers with provisional TCGA data): frequency of expression alterations (%) in genes from COX-2-PGE_2 pathway and correlation to survival (Logrank test p-value).

Cancer type	**n**	**PTGS2**	**PTGES**	**PTGES2**	**PTGES3**	**PTGER1**	**PTGER2**	**PTGER3**	**PTGER4**	**OS**	**DFS**
Adrenocortical ca.	79	1.3	4	5	19	9	1.3	5	6	0.181	0.130
Cholangiocarcinoma	36	6	6	6	2.8	8	2.8	2.8	2.8	0.322	
Bladder urothelial ca.	408	4	3	2.5	8	5	3	4	8	0.0702	
Colorectal adenoca.	379	3	6	1.6	7	2.4	4	4	4	0.0375	
Breast invasive ca.	1093	1.7	4	4	8	1.6	2.6	2.8	3	0.259	
Glioblastoma mult.	160	3	6	6	8	6	4	6	3		
Cervical SCC	304	2.6	6	4	9	5	4	8	6	0.17*	
Esophageal carcinoma	184	7	2.7	8	8	5	6	1.6	9		
Stomach adenoca.	415	5	4	9	9	4	0.7	4	7		0.09*
Uveal melanoma	80	5	2.5	6	6**	5	5	5	5		
HNSCC	520	2.3	4	7	7	2.5	4	3	6	0.090	5.693 e-3
Kidney renal clear cell ca	533	1.3	2.3	2.4	5	0.4	4	7	5	0.179	0.144
Kidney renal papillary cell ca.	290	2.4	4	4	9	3	4	2.4	4	0.034	0.307
Liver hepatocellular ca.	371	0.8	6	7	8	6	3	1.3	4	0.283	
Lung adenocarcinoma	515	4	4	3	11	2.1	5	3	4	0.039	
Lung SCC	501	4	6	3	5	2.4	1.2	1.4	7		0.202
AML	173	4	5	4	2.9	2.3	3	2.9	2.3		n/a
Ovarian serous cystadenoca.	307	0.7	2.6	7	4	2.3	2	5	5	2.305 e-3	0.286
Pancreatic adenoca.	178	4	4	1.7	10	3	4	6	4	0.089	0.080
Mesothelioma	87	3	1.1	1.1	10	8	1.1	3	5	n/a	n/a
Prostate adenoca.	497	2.8	5	6	5	4	4	5	3		0.262
Skin cutaneous melanoma	469	8	1.7	3	9	4	4	2.1	3	0.118	0.236
Sarcoma	259	5	10	6	8	5	8	4	5		
Testicular germ cell ca.	150	2	7	7	9	5	6	3	3		0.072
Thymoma	120	5	3	3	8**	4	4	3	4	0.017	0.290
Thyroid cancer	501	3	2.4	4	6	3	3	3	5		
Uterine corpus endothelial carc.	177	1.7	2.8	5	6	4	7	3	6		
Overall %		**3.4**	**4.3**	**4.7**	**7.7**	**4.1**	**3.7**	**3.7**	**4.8**		

OS, Overall Survival, DFS, Disease/Progression Free Survival. Only p-values < 0.35 are shown. OS and DFS values describe negative impact on survival, unless marked by * (correlation with better survival). Expression alterations are predominantly observed as overexpression unless marked by ** (where downregulation is observed). SCC, squamous cell carcinoma.

Table S6. cBioPortal RNA-seq data (for cancers with provisional TCGA data): frequency of expression alterations (%) in genes involved in glutathione synthesis and correlation to survival (Logrank test p-value).

Cancer type	**n**	**GCLC**	**GCLM**	**GSS**	**GGCT**	**OPLAH**	**GSR**	**OS**	**DFS**
Adrenocortical ca.	79	5	1.3	6	16	6	4	0.093	
Cholangiocarcinoma	36	8	2.8	2.8	11	8	6		0.296
Bladder urothelial ca.	408	4	4	18	16	11	2.9	6.327 e-3	0.231
Colorectal adenoca.	379	8	4	39	20	7	16**		
Breast invasive ca.	1093	5	7	10	8	15	4	0.017	0.339
Glioblastoma mult.	160	4	4	14	31	3	8	0.175	0.087
Cervical SCC	304	3	3	12	8	8	4		
Esophageal carcinoma	184	7	4	13	16	11	8		
Stomach adenoca.	415	7	6	14	13	15	9	0.04*	0.163*
Uveal melanoma	80	13	1.3	8	6	35	6		
HNSCC	520	6	6	10	8	12	6	0.019	2.763e-3
Kidney renal clear cell ca	533	5	4	6	8	5	5	0.185	0.070
Kidney renal papillary cell ca.	290	4	4	16	7	8	3	0.051	0.041
Liver hepatocellular ca.	371	6	3	5	7	20	2.7		
Lung adenocarcinoma	515	6	2.9	8	5	14	5	0.035	
Lung SCC	501	7	7	10	10	12	5		0.211*
AML	173	5	6	4	3	6	7		
Ovarian serous cystadenoca.	307	4	4	13	4	35	3		0.337*
Pancreatic adenoca.	178	4	2.2	8	7	7	5	0.15*	
Mesothelioma	87	7	3	6	3	9	6	n/a	n/a
Prostate adenoca.	497	6	4	4	8	11	6**	0.13*	7.141e-3
Skin cutaneous melanoma	469	13	5	11	18	8	8	2.585 e-3	0.184
Sarcoma	259	2.7	4	9	12	3	5	0.011	0.041
Testicular germ cell ca.	150	7	13	2.7	26	4	9 **	0.05	
Thymoma	120	6	3	7	6	4	5	1.111 e-4	
Thyroid cancer	501	2.4	1.8	6	4	1.4	1.6		
Uterine corpus endothelial carc.	177	5	4	6	6	12	3		
Overall %		**5.9**	**4.2**	**9.9**	**10.6**	**10.8**	**5.7**		

OS, Overall Survival, DFS, Disease/Progression Free Survival. Only p-values < 0.35 are shown. OS and DFS values describe negative impact on survival, unless marked by * (correlation with better survival). Expression alterations are predominantly observed as overexpression unless marked by ** (where downregulation is observed). SCC, squamous cell carcinoma.

Table S7. qRT-PCR primers' sequences.

Gene	Forward (5'-3')	Reverse (5'-3')
DNMT1	GAGCCACAGATGCTGACAAA	GACACAGGTGACCGTGCTTA
DNMT3A	AAGGAGGAGCGCCAAGAG	GGATGGGGACTTGGAGATCA
DNMT3B	GGGAGGTGTCCAGTCTGCTA	GGCTTTCTGAACGAGTCCTG
TP63	GTTTCGACGTGTCCTTCCAG	TCTGGATGGGGCATGTCTTT
KRT5	TGAGGTCAAGGCCCAGTATG	ATCTCATGCTTGGTGTTGCG
IVL	AACACAAAGGGATCAGCAGC	GCTCCAACAGTTGCTCTTTCT
PTGS2 (COX-2)	TCATCATCAGCGCCCTCAA	GCTCGTTCACAGCCTTCATG
PTGER1 (EP-1)	GCCAGCTTGTCGGTATCATG	CTGCAGGGAGGTAGAGCTC
PTGER2 (EP-2)	AAGCTGTGGTCAAGGCTACA	GCCAAGTACCATGCTCACTG
PTGER3 (EP-3)	GGATCATGTGCGTGCTGTC	TGTGTCTTGCAGTGCTCAAC
PTGER4 (EP-4)	TGCTCATCTGCTCCATCCC	ATTCGGATGGCCTGCAAATC
ALOX5	ACATCTACCTCAGCCTCGTG	AGTTCCTCGTCCACAGTCAC
ALOX15B	AAATCAAGGGGTTGCTGGAC	AACTGGGAGGCGAAGAAGG
ALOX12	CTTGCTGAACACTCACCTGG	ATGGTGTAGCGGATATGGGG
LTA4H	GACTTCTGGGAAGGAACACC	TGCCACCAGTTCTTTAGGGA
CYP2E1	CGGAACTATGGGATGGGGAA	CGGAAGAGGATGTCGGCTAT
ITGAM (CD11b)	TGTTTCACGGAACCTCAGGA	ATCCATTGTGAGGTCCTGGC
ACTB	AAAGACCTGTACGCCAACAC	GTCATACTCCTGCTTGCTGAT